5-2018

The Use of Mixed Organic/Ionic Liquid Electrolytes with Forcespun Metal Oxides/Carbon Microfiber Electrodes in Lithium Ion Batteries

Jahaziel Villarreal
The University of Texas Rio Grande Valley

THE USE OF MIXED ORGANIC/IONIC LIQUID ELECTROLYTES WITH FORCESPUN METAL OXIDES/CARBON MICROFIBER ELECTRODES IN LITHIUM ION BATTERIES

A Thesis

by

JAHAZIEL VILLARREAL

Submitted to the Graduate College of
The University of Texas Rio Grande Valley
In partial fulfillment of the requirements for the degree of

MASTER OF SCIENCE ENGINEERING

May 2018

Major Subject: Mechanical Engineering

THE USE OF MIXED ORGANIC/IONIC LIQUID ELECTROLYTES WITH FORCESPUN METAL OXIDES/CARBON MICROFIBER ELECTRODES IN LITHIUM ION BATTERIES

A Thesis
by
JAHAZIEL VILLARREAL

COMMITTEE MEMBERS

Dr. Mataz Alcoutlabi
Chair of Committee

Dr. Karen Lozano
Committee Member

Dr. Jose Gutierrez
Committee Member

Dr. Maysam Pournik
Committee Member

Dr. Rogelio Benitez Jr.
Committee Member

May 2018

ABSTRACT

Villarreal, Jahaziel, The Use of Mixed Organic/Ionic Liquid Electrolytes With Forcespun Metal Oxides/Carbon Microfiber Electrodes in Lithium Ion Batteries. Master of Science Engineering (MSE), May, 2018, 67 pp, 48 figures, references, 47 titles.

Ionic liquids (ILs) are regarded as an alternative electrolyte for the current generation of lithium ion batteries (LIBs). This research work examines mix organic/ionic liquid electrolyte (MOILEs) and the addition of succinonitrile (SN) as an additive with alternative carbon nano fiber (CNF) anode and cathode. ILs are non-flammable, have high flash points, and low volatility this characteristics would enhance safety parameters that are absent in organic liquid electrolytes (OLEs). Though there are still going to be organic electrolyte due to electrochemical characteristics that ILs do not have it would be less and would be non-flammable.

DEDICATION

To whom believed in me and the Logos.

ACKNOWLEDGMENTS

My academic success could not have been possible if the right people had not guided me. My appreciation goes towards my PI, Dr. Mataz Y. Alcoutlabi for allowing me to be part of his battery research group and being the chair of my thesis committee. To my four committee members: Karen Lozano, Jose Gutierrez, Mayasam Pournik, and Rogelio Benitez for their time and effort invested on me, but also on the Rio Grande Valley community. My achievement is not mine, but the whole battery research group that are or were part of the laboratory (Post Docs, graduates and undergraduates). Finally, to Hilario Cortez and Alejandro Castillo, for helping me with the SEM/EDS characterization techniques. This project would have not been available to be accomplished without the funding supported by NSF PREM award under grant No. DMR-1523577: UTRGV-UMN Partnership for Fostering Innovation by Bridging Excellence in Research and Student Success.

TABLE OF CONTENTS

LIST OF FIGURES

CHAPTER I

INTRODUCTION

Electrochemical energy storage technologies are in high demand due to long cycle life, and low maintenance. Based on energy density and the nature of their electrochemical performance, lithium-based batteries were proposed due to their light weight, reduced volume, and high energy density. A lithium battery (LB) consists of a lithium metal as the anode. LB is a primary battery that is non-rechargeable, does not go through irreversible reaction, has a long shelf life, and has a high specific capacity [1-3]. A Lithium-ion battery (LIB) consists of a lithium metal oxide (LMO) as the cathode and graphite as the anode, where the energy is stored via a reversible intercalation reaction from cathode to anode. LIBs are secondary batteries with a reversible reaction, are rechargeable, have long shelf life, and high specific capacity. Secondary batteries gained popularity in 1991 and quickly became the apex for rechargeable battery applications. Their main use in the mobile phone industry experienced an exponential success in the energy storage industry [4, 5]. Due to its unmatched energy and power density, much slimmer and smaller mobile phone designs were achieved, opening broader market opportunities. This battery chemistry is used in electric vehicles, being the perfect candidate for this application, and could replace fossil fuels in the automobile industry [6, 7]. There are different safety issues that LIBs must overcome. The current generation of electrolytes in LIBs utilizes a mixture of organic carbonates that are highly volatile and flammable. These solvents are currently used due to their solubility for the lithium salts and low viscosity allowing lithium ion

diffusion. Despite these advantages, the organic liquid electrolytes (OLEs) present safety disadvantages. This includes inadequate oxidative stability when cycled at high voltage, high volatility, flammability, leakage from the cell, and a narrow working temperature range. Since LIBs work in oxidation/reduction reaction, the cathode and anode must also be chemically stable in OLEs. There are different electrode materials with a wide variety of range in voltage that would have to be safe to be used with organic liquid electrolytes. The following section focuses on a pertinent literature review to discuss the various aspects of electrolytes used in LIBs and their mixture with different additives with the aim to improve the electrochemical performance and safety of LIBs.

CHAPTER II

LITERATURE REVIEW

2.1 Electrolyte Overview

The nature of the electrolyte and the electrode physical state is an important role in determining the electrochemical performance and stability of LIBs. The electrolyte is the medium in which the lithium ion (Li^+) is transported from cathode to anode during charging (Li-insertion), and from anode to cathode during discharge (Li-deinsertion). There are different commercial electrolytes available including organic liquid electrolytes (OLEs), ionic liquid electrolytes (ILEs), and solid electrolytes (SEs) [8, 9]. OLEs are used commercially and consist of mixed organic carbonates with a lithium salts such as, lithium tetrafluoroborate ($LiBF_4$), titanium triflate lithium perchlorate ($TiLiClO_4$), lithium hexafluoro-arsenate (LiAsF6), and more commonly, lithium hexafluorophospate ($LiPF_6$). The stability of the alkyl carbonates with $LiPF_6$ salt was chosen due to the permeability, cathodic/anodic stability, ionic conductivity, and low viscosity[10]. A lithium metal oxide (LMO) cathode provides Li^+ that is transported through the electrolyte passing through the separator and intercalating into the graphite anode. The separator is located between the anode and the cathode to prevent physical contact and avoid any short circuits. These separators consist of a polymer such as polypropylene (PP), and polyethylene (PE) or ceramic materials that are semi-permeable for lithium ion diffusion and chemically resistant to solvents found in the electrolyte, however, it decreases ionic conductivity (Figure 1).

Ionic conductivity is the measurement of the movement of Li^+ from the cathode to the anode and vice versa via an aqueous solution. It is worth mentioning that the organic carbonate component plays an important part in the formation of solid electrolyte interface (SEI), which is a passivation film formed at the anode surface. Proper SEI formation is crucial as this passivation layer efficiently intercalates the Li^+ to the graphite structure. Both the cathode and the anode have a metal current collector (aluminum for cathode and copper for anode). For this reason, the electrolyte must be chemically stable to avoid any corrosion during charge/discharge cycles.

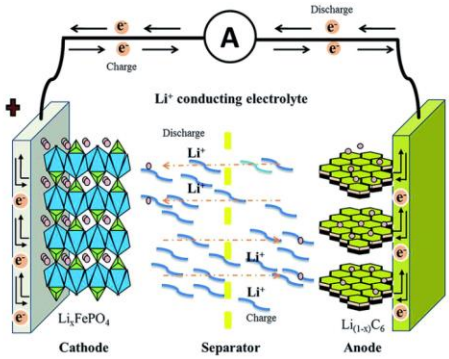

Figure 1: Schematic of a lithium ion battery and the working principal [11].

Despite having all components required, organic electrolytes have safety issues. These issues are caused by the volatility, flammability, and low temperature functioning window. Market demands for LIBs call for, higher power density and energy, however, these requirements do not meet the safety parameter due to the issues previously mentioned. Research conducted on alternative electrolytes includes the following: solid electrolytes, ionic liquids, and hybrid electrolytes.

2.1.1 Additives

Electrolytes mixed with a small quantity of additives improved electrochemical performance of the battery. The characteristics of additives include SEI formation, cathode

protecting agents, $LiPF_6$ salt stabilizers, safety protection agents, and improvements of ionic conductivity[12]. The most commonly used additive to improve the SEI formation is flouroethylene carbonate (FEC). Results reported in literature show that the addition of FEC to a liquid electrolyte leads to improved SEI layer formation caused by the bonds between the halogen species that reduce the electrolyte [13, 14]. The deterioration of the cathode is caused by the irreversible oxidization of the electrolyte, acidity impurities, and water. N,N-diethylamino trimethylsilane is an additive composed of water and HF acid scavenger which can reduce the deterioration of the aluminum current collector and the cathode material. $LiPF_6$ salt is highly reacted in constant decomposition from $LiPF_6 \Leftrightarrow PF_5 + LiF$. The PF_5 by product is highly reactive with the organic solvent and deteriorates the SEI layer. Research has been performed on amide-based compounds, demonstrating that the delocalized electron withdrawing groups are weak bases reducing or eliminating the reactivity of PF_5 [9]. Safety protecting agents could include overcharge or fire-retardant additives. To counteract any overcharge, additives such as xylene, cohyxylbenzine and 3-thiopheneacetonitrile can polymerize realizing gas. This would activate a current interrupt device (CID) located in high capacity LIBs [15]. Fire retardant additives consist of organic phosphorous compounds. This mechanism goes through a halogenated derivative which reduces the free radicals formed by the decomposition of $LIPF_6$ [16]. To increase lithium ion transport in organic liquid electrolytes, a borate compounds that are electron-deficient were used as additives. Tris(pentafluorophenyl) borane (TPFPB) resulted in an increase of electrolyte retention in the separator allowing lithium ions to easily flow from the cathode side to the anode and vice versa [17].

Succinonitrile (SN) has been used in super capacitors, fuel cells, solar cells and LIBs. SN has been also used as an additive in LIBs to improve the thermal stability, cycling performance,

reduce impedance and improve SEI formation [18-20]. High voltage cathodes present safety problem for LIBs and are prone to thermal runaway. Using $LiPF_6$ as a salt in OLEs can produce $LiPF_6$ hydrolysis products such as HF in the presence of trace amount of moister impurities in the electrolyte that evolve during lithium-ion battery cell operation at elevated operation temperatures and high operation voltages [21]. Nitriles such as SN can react with the HF and water impurities, which can stop or reduce the process of $LiPF_6$ decomposition and hence improve the thermal stability of the battery. The addition of 1 wt% of SN to the electrolyte has resulted in the improvement of the cycling performance and thermal stability of high voltage cathode materials [22].

2.1.2 Ionic Liquids Electrolytes

Ionic liquids (ILs) are composed of ions, a positive charge (cation) and a negative charge (anion), which is a characteristic of a salt. However, a conventional ionic salt (solid) has highly organized ions that form a crystalline lattice. Despite having characteristics of a salt, ILs are liquids at room temperature, which is attributed to the disorganization of ions as demonstrated in Figure 2. The ILs show more flexibility or mobility to host ions such as Li^+ in contrast with ionic solids. This mobility will allow the Li^+ to flow more at ease, having less resistance, increasing ionic conductivity. [23-26].

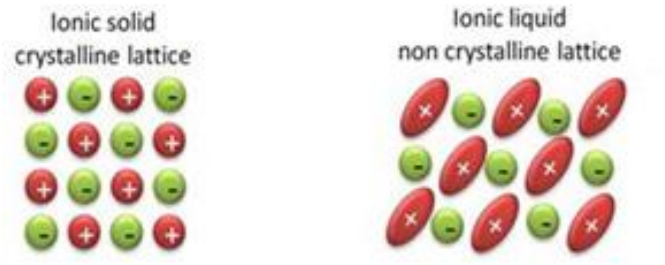

Figure 2: Comparison of the crystal structure of ionic solids and ionic liquids [27].

The most commonly used families of ILs are imidazolium, piperidiunium, and pyrrolidinium. These ILs are non-volatile, non-flammable, have a wide electrochemical window and hi voltage, and are liquids over a wide temperature range, making them a suitable, safe and green electrolyte alternatives [28-31]. The synthesis procedure must yield a high purity in order to maintain the necessary requirements for an electrochemically stable battery. Ionic liquids are made completely out of ions; they are viscous at room temperature and exhibit a low ionic conductivity. As the temperature increases, the viscosity decreases, therefore, the ionic conductivity increases exponentially [32]. The IL with the least viscosity is imidazolium, which also has a good solubility characteristic for lithium salts. When the lithium salt is dissolved in the IL, it becomes an ionic liquid electrolyte (ILE). ILEs require the formation of a SEI layer in the anode through the decomposition of the Li salt and solvent. However, ILEs have unstable chemical decomposition and are not prone to form thin morphological consistent SEI layer. Furthermore, the viscosity of ILEs must be low for the Li ions to flow and diffuse faster into the anode to intercalate/de-intercalate with graphite during the discharge and charge processes.

2.1.3 EMI-TFSI

The melting point of an ionic liquid is determined by the interactions of cations and anions. Each IL has a different chemical and physical characteristic depending on the structure and size of the cation and anion. In the imidazolium family, an IL that has gained significant attention is ethyl-methyl-imidazolium, bis-(trifluoromethanesulfonyl)-imide (EMI-TFSI) due to its low viscosity, high ionic conductivity, melting point of -16 °C, and decomposition temperature of 455 °C [33]. As demonstrated if Figure 3 the cation and anion of EMI-TFSI have unsymmetrical structures which does not allow for orderly crystal formation.

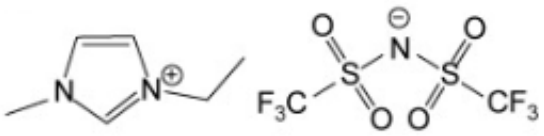

Figure 3: Molecular structure of EMI-TFSI [34].

The EMI cation is limited by the electrochemical reduction and the oxidation. However, TFSI anion was proposed and successfully used in ILEs due to its high anodic stability, good conductivity, excellent thermal stability and hydrophobicity which prevents hydrogen bonding. The TFSI anion can improve the cycle ability and long-term stability of LIBs [35]. In order for EMI-TFSI to be used as an IL electrolyte, it requires a lithium salt that could be dissolved in it. A chemically stable and soluble salt in EMI-TFSI is Lithium bis(trifluoromethanesulfonyl)imide (LiTFSI) which exhibits favorable transport properties needed for Li^+ to transport in the electrolyte during the charge/discharge process. Despite the qualities of EMI-TFSI, there are still limitations that need to be overcome in order to use EMI-TFSI as a suitable electrolyte in LIBs.

2.1.4 Mixed Organic/Liquid Electrolytes (MOILEs)

The chemical structure of ILs gives advantages and disadvantages for using as electrolyte. Both anion and cation are large, making them viscous, leading to low ionic conductivity, having unstable SEI layer formation due to the chemical decomposition of the IL on the graphite anode, which have restrained the use of ILs in LIBs[36]. A method used to counteract those two disadvantages is mixing organic carbonate solvents with ILs. This would reduce the viscosity, increase the ionic conductivity and decompose the organic solvent to produce a thin morphological uniform SEI layer. Studies on anodes have demonstrated that the addition of 40% EMI-TFSI in the organic electrolyte successfully improved the Li^+ diffusivity, SEI formation and cycle performance [37]. *An et al*. provided a mixture ratio of 6:4 of IL to

organic solvent that resulted in a good thermally stability of the electrolyte. The mixed electrolyte also showed high ionic conductivity, and good electrochemical performance of lithium iron phosphate ($LiFePO_4$) cathode [38, 39]. Mixed organic/liquid electrolytes (MOILEs) have a broad generalization and some properties have been investigated for a set of electrodes to a specific IL. The solubility of ILs in organic liquid electrolytes plays a very important role to determine the viscosity of MOILEs[40]. The addition of additives such as SN could also improve the MOILEs electrochemical stability and the battery performance, depending on the electrolyte characteristics. The present work focuses on the effect of SN content on the electrochemical performance and stability of MOILEs in LIBs.

2.2 Anode Overview

Graphite is the commercial anode used in LIBs. It is an allotrope of carbon that has good performance, is reliable, inexpensive, and safe. Graphite is layered hexagonally bonded structure sheets of carbon allowing lithium ions to be inserted or intercalated between the two planes of graphite and in the six carbon atoms, as demonstrated in Figure 4. A Li^+ could only be inserted between every other carbon hexagonal sheet having one lithium ion to every six carbon atoms[41].

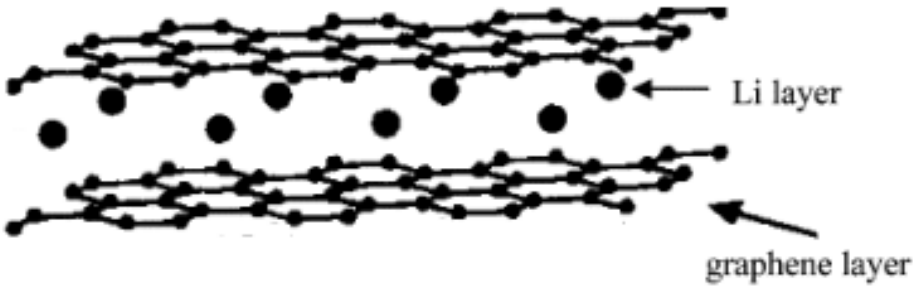

Figure 4: Two graphite layers with an intercalated lithium ion [42].

This is attributed to the energy storage density of graphite having a theoretical capacity limit of 372 $mAhg^{-1}$, with the following reduction reaction:

$$xLi^{+} + xe^{-} + \leftrightharpoons Li_xC_{6.}$$

These properties have minimal impact on the volume expansion of the crystal structure and reduce the stresses and strains. The low volume expansion of the crystal structure maintains a long charge-discharge capacity, cycle life efficiency with high coulombic efficiency. A commercial anode is fabricated by shear mixing the active material graphite, conductive filler carbon black and a polymer binder. The mixture is diluted with an organic solvent to form a slurry with an ink like consistency. This slurry is then used to coat a copper current collector, which is dried and used as anode. Drawbacks for graphite anodes are that they exhibit low energy density, are prone to pulverization and have a non-conductive binder that could reduce the ionic conductivity and battery capacity [43, 44].

2.2.1 Metal/Alloy Based Anodes

Metals based anodes exhibit greater theoretical capacity than graphite anode. For example, anode materials such as lithium aluminum (LiAl) with a theoretical capacity of antimony (Sb), silicon (Si) tin (Sn) of 994 $mAhg^{-1}$, 536 $mAhg^{-1}$, 3600, and 994 $mAhg^{-1}$, respectively of. The reason for these anodes to have high theoretical capacity is that these metals undergo two different types of reaction, alloying/di-alloying and insertion/di-insertion reactions. These metals could store more lithium ions than a conventional graphite anode because they form an alloy and having higher storing capability. The insertion capacity of these metals could be of 2-4 lithium atoms per every 6 carbon atoms (graphite can only hold 1 lithium atom for every 6 carbon atoms). Some metal oxides (e.g. Fe_2O_3, SnO_2, and MoO2) not only have better

power and energy density, but they also are abundant, inexpensive, and environmentally friendly. However, increasing the lithium ion capacity will induce higher volume expansion up to 500%. This would produce pulverization of the material due to the high stresses and strains as showed in Figure 5. Once pulverization occurs, each cycle would be losing a fraction of the capacity having a linear degradation. There are new methods to be explored to reduce the volume change and maintain the desired electrochemical characteristics.

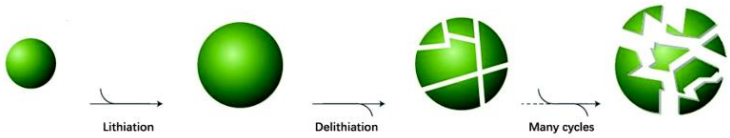

Figure 5: The pulverization mechanism of metal alloy atoms [45].

Metal/alloy based anodes could be produced in numerous methods such as composites, nanocomposite, and composite/carbon nanofibers. Most composites are produced by mixing a metal powder with conductive carbon, then placed in a furnace at the temperature in which the metal melts. The melted metal will adhere to the carbon, and cool to form a metal carbon composite. Nanocomposite include egg yolk, nano wires, and nano sheet structures restraining the full expansion of the metal avoiding maximum stress in the material that will reduce pulverization [46-48]. Composite/carbon nanofibers are produced by adding metal active material into a solution that would produce fibers by electrospray, touch brush spinning, electrospinning and force spinning [11, 49-52].

2.2.2 Forcespinning

The production of carbon fibers (CFs) can be obtained through different methods such as liquid shearing, electrospray, electrospinning, and centrifugal spinning. The most used method to

produce fibers and nanofibers is electrospinning. In this method, 40 kVs are applied to a polymer solution that becomes charge and electrostatic repulsion acts against the surface tension. The electrostatic repulsion can cause a whipping process, which forms jet streams of fibers that are directly deposited on the ground collector. *Sarkar et al.* developed the Forcespining® method through the centrifugal spinning [53-55]. In contrary to the other methods, Forcespinning® can produce a wider variety of CFs, because it does not require a di-electric solution. This technique produces fibers by stretching a polymer solution, which is injected into a rotating reservoir that would be spun using centrifugal forces as shown in Figure 6. The Forcespining® method has a high yield of fibers in comparison with the previous techniques. This method is not subjugated to making mono-polymer fibers; it is also capable of producing co-polymers due to the continuous injection of the solution. It could also do melt spinning at temperatures as high as 350 °C which would reduce or eliminate the presence of a solvent. These fibers can be used in several different industries such as clothing, medical, filtering, and energy storage.

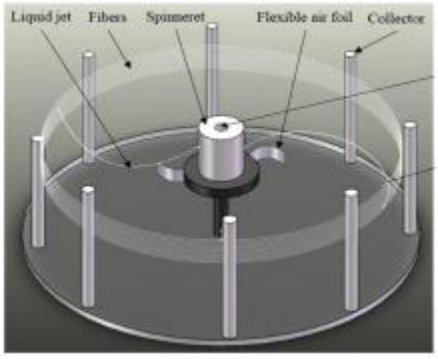

Figure 6: Schematic of fiber production through centrifugal forces [56].

2.2.3 Carbon Fibers as Anodes

Electrospinning is the most used method to prepare carbon fibers **(**CFs**)** as electrode materials in energy storage devices. The Forcespining® method has revolutionized the CFs

research, since it is an alternative to electrospinning. Due to the high yield, it is a reasonable method to use and produce fibers for anodes or cathodes. The fibers produced through the Forcespining® method are composed of a polymer that could be thermally treated and transformed into CFs. In contrary to graphite, the CFs do not contain a non-conductive binder, are flexible and have high surface area to volume ratio (they are considered as binder-free anodes or free-standing anodes). These qualities are gaining interest due to the new applications used in electronic devices. In addition, metal oxide nanoparticles could be introduced in the fibers obtaining the electrochemical advantages of the metal oxides, increasing capacity, and using a fully conductive material (CFs).

2.3 Cathode Materials Overview

Lithium cobalt oxide ($LiCoO_2$) was the first commercially cathode material used in LIBs. $LiCoO_2$ has a high specific energy density due to the layered structure of the CoO_2, where the lithium ion could readily be inserted and di-inserted during the charge and discharge cycles, as showed in Figure 7. The theoretical capacity of $LiCoO_2$ is 273 $mAhg^{-1}$, and has a working capacity of 145 $mAhg^{-1}$.

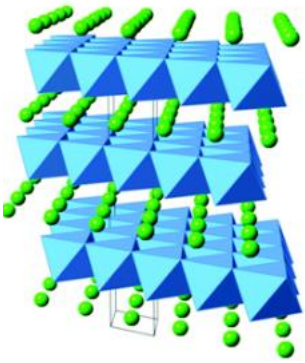

Figure 7: Crystal structure or $LiCoO_2$ [57].

However, there has been numerous works done to design alternative cathode materials for LIBs, and new materials have been researched and used as cathodes for LIBs. The following criteria are taken into consideration when designing a new cathode material: specific energy, specific power, safety, performance, life span, and cost. Since then, the cathode materials used have been, lithium manganese oxide ($LiMn_2O_4$), lithium nickel manganese cobalt oxide ($LiNiMnCoO_2$), lithium titanate ($Li_4Ti_5O_{12}$), and lithium iron phosphate ($LiPO_4$). The method of producing cathodes (slurry) includes the active material (lithium metal molecule), the conductive filler (carbon black) and a polymer binder. The polymer is a non-conductive reducing agent.

2.3.1 Lithium Iron Phospate

$LiPO_4$ is a lithium metal oxide that is more tolerant, undergoes less stress in the system and keeps voltage for longer time. The crystal structure of the $LiFePO_4$ demonstrates how the lithium is organized (Figure 8) being similar to $LiCoO_2$. However, it has similar specific capacity, is low in cost, and has safer parameters [58].

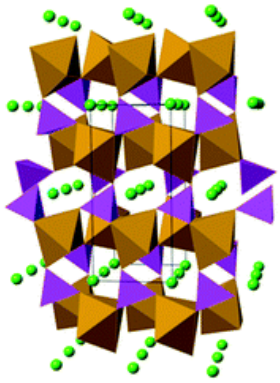

Figure 8: Crystal structure of $LiFePO_4$ [57].

The theoretical capacity of LiFePO4 is 173 $mAhg^{-1}$, with a working capacity of 140 $mAhg^{-1}$. As observed, the working capacity of $LiCoO_2$ and $LiFePO_4$ are similar. However, the thermal runaway temperature of $LiCoO_2$ is 150 °C as compared to the temperature of $LiFePO_4$ (270 °C)

[59]. Considering that the electrolyte is highly volatile, this safety parameter plays an important role in replacing $LiCoO_2$ with $LiFePO_4$. $LiFePO_4$ particles could also be induced in CFs to produce composite cathodes and could be an alternative for the conventional slurry method such as mentioned for the anodes [60, 61].

CHAPTER III

EXPERIMENTAL PROCEDURE

3.1 EMI-TFSI

The following analytical grade reagents were purchased for the synthesis of ILs and MOILEs. Bis(trifluoromethane)sulfonimide lithium salt 99 % (Li-TFSI) and 1-Ethyl-2,3-methylimidazolium bromide 99.98% (EMI-Br) were purchased from Io-li-tech USA. HPLC water, silica oxide, and sand were obtained from Sigma-Aldrich. The organic solvents used, ethylene carbonate (EC) (99%) and dimethyl carbonate (DMC), were purchased from Alpha Aesar chemical company and Fisher Scientific, respectively. LiTFSI (98%) and dichloromethane (DCM) (99%) were purchased from Sigma-Aldrich.

3.1.1 Synthesis of EMI-TFSI

A 1:1 stoichiometric ratio of LiTFSI to EMI-Br was reacted by adding sufficient HPLC water into a 500 mL round bottom flask containing the reagents and stirred for 24 hours at 70 °C in an oil bath. The reaction would form two layers, the aqueous and the ionic liquid (EMI-TFSI), then it was taken out of the oil bath to cool down to room temperature. Then, EMI-TFSI was washed with HPLC water using the following steps. The EMI-TFSI was separated from the aqueous solution and decanted into a separator funnel. HPLC water was then poured into the separator funnel where the EMI-TFSI was located and was vigorously mixed. The separator funnel was then placed in a ring stand to rest form a minute until the two layers were formed, the

washing process was then repeated three times. The EMI-TFSI was placed in the 500 mL round bottom flask, then dissolved with sufficient DCM.

A chromatography column with a 500 mL reservoir was used. The column filled first with 1 inch of sand followed by the silica oxide all the way to the top before reaching the reservoir. DCM was then decanted to the column to wet the silica oxide.

The EMI-TFSI dissolved in DMC contained in the 500 mL round bottom flask was decanted to the chromatography column. The column was then drained into a round bottom flask. This purpose of this process is to filtrate any impurities left in the EMI-TFSI.

The solution in the 500 mL round bottom flask was put into a Rota Vapor removing excess water. The Rota Vapor had a temperature of 90 °C and rotated at 40 rpm. The DCM solvent was collected in the trap, which was later discarded in the organic waste container. The EMI-TFSI was left in the 500 mL round bottom flask.

The 500 mL round bottom flask containing the EMI-TFSI was then put under vacuum at a temperature of 100 °C for 48 hours to remove any water and DCM. After 48 hours, the EMI-TFSI was immediately transferred to a glove box that is under Argon atmosphere with <0.5 ppm of O_2 and <0.5 ppm of H_2O. EMI-TFSI had a density of 1.53 mg/cm^2, consistent with results reported in the literature.

3.1.2 Preparation of MOILE

The preparation of MOILEs was performed inside a glove box under Argon atmosphere. A 20 mL solution of EC and DMC was prepared. EC was dissolved into DMC with a 1:1 v/v ratio and then mechanically stirred for 2 hours, having a final density of 1.282 mg/cm^2.

Batches of 5 mL 1 M of LiTFSI in 60% EMI-TFSI and 40% EC/DMC were prepared. Lithium salt was added in a 20 mL disposable glass vile with a micro magnetic stir bar 1.435 g of LiTFSI, followed by 2.564 g of EC/DMC solution, after the LiTFSI salt was fully dissolved; 4.590 g of EMI-TFSI were added and stirred for 24 hours. The EC/DMC and the EMI-TFSI were weighed because of viscosity of the IL, however, the final volume was 5 mL, having a total mass of 8.590 g. Finally, an additional 0.429 g of SN were added, constituting 5 wt%.

3.1.3 Preparation of OLE

The OLE, prepared in the laboratory, consisted of EC/DMC and $LiPF_6$ as the lithium salt. Batches of 40 mL of OLE were prepared by magnetically stirring for 2 hours in a 1:1 v/v ratio of EC to DMC, then an amount of 6.07 g of $LiPF_6$ was added to form a 1 M electrolyte solution. The electrolyte was left to stir overnight before used.

3.2 Fabrication of Fibers

The following chemicals were purchased in order to synthesize and produce the CFs. Poly(vinylpyrrolidone) (PVP) with average molecular weight (Mw) of 180,000, polyacrylonitrile (PAN) with average Mw of 150,000, and polyacrylic acid (PAA) were purchased from Sigma-Aldrich. Dimethylformamide (DMF) (>99.5%), ethanol (200 proof), Tin (II) 2-ethylhexaonate

were purchased from Fisher Scientific. Lithium iron phosphate powder was purchased from MTI Corps. All chemicals were used as received.

3.2.1 Preparation of Carbon Fibers

CFs were prepared by mechanically mixing and dissolving 12 wt% of PAN into DMF for 24 hours. CFs were produced by injecting 2 mL of the 12 wt% PAN solution into the spinneret of the Cyclon L-1000. The spinneret was fitted with 30-gauge half-inch needles and spun for one minute under 8000 rpm, producing fiber jets. The PAN fibers were deposited and collected on a polypropylene substrate forming a fibrous mat. The fibrous mat was removed from the substrate and dried under vacuum at a temperature of 100 °C for 24 hours. The PAN fibers were then put into OTF-1200X tube furnace, purchased from MTI, and stabilized under air at 280 °C for 5 hours at a rate of 3 °C/min, and subsequently carbonized under Argon atmosphere at 700 °C for 3 hours using the same heating rate [62]. After removing the CFs from the furnace, they were punched to a ½ inch diameter disc, weighed and used as anodes for half Li-ion cells.

3.2.2 SnO_2/ Carbon Composite Fibers

The SnO_2/C composite fibers were prepared by dissolving 12 wt% of PAN in ethanol. The PAN/ ethanol solution was mechanically mixed using a magnet rod on a stirring plate for 2 hours at 25C to obtain a homogeneous solution. Tin (II) 2-ethylhexanoate solution was added to a 2:1 weight ratio of PAN and left to stir for 24 hours. The PAN/Sn precursor fibers were produced by the Forcespining of PAN/Sn solution A 2 mL of the solution was inserted into the base spinneret containing a 30 gauge half-inch needle. The solution was then spun in the L1000 cyclone at a rotational speed of 8,000 rpm for one minute. The polypropylene substrate collector was then used to collect the PAN/Sn fibers by rotating the substrate 90° at each run. The 4"x4 "

fibrous mat was removed from the substrate and then was vacuum dried at 100 °C for 24 hours. The SnO_2 fiberous mat was carbonized in the OTF-1200X tube furnace. The carbonization treatment of SnO_2 was performed exactly as the CFs. Being stabilized under air at 280 °C for 5 hours at a rate of 3 °C/min, and subsequently carbonized under Argon atmosphere at 700 °C for 3 hours using the same heating rate. The SnO_2/C composite were removed from the furnace, punched to a ½ inch diameter disc, then weighed and used as anodes for half Li-ion cells.

3.2.3 $LiFePO_4$/ Carbon Cathodes

A slurry (paste) of $LiFePO_4$ /carbon composite was prepared by dissolving 15 wt% of PVP in ethanol using mechanical stirring for 6 hours to obtain a homogeneous solution. $LiFePO_4$ powder was added in a 2:1 ratio to PVP solution. The $LiFePO_4$/PVP/ethanol solution was vigorously mixed using a magnetic stirring rod at room temperature for 24 hours.

The prepared solution was forcespun using the L1000 cyclone by injecting 2mL into the spinneret where the temperature in the laboratory was 22 °C in a 45% humidity. The spinneret was equipped with 30-gauge half-inch needles and spun with a rotational speed of 8500 rpm for one minute. The fibers were collected using a 4"x4" polypropylene substrate and then put under vacuum at 100 °C for 24 hours. The dried fibers were carbonized using the following thermal history, stabilization at 200 °C for 5 hours at a rate of 3 C°/min under air, then carbonized at 550 °C for 3 hours using the same heating rate.

A binder solution was prepared by adding 7 wt% of PAA to ethanol solvent. $LiFePO_4$/carbon fiber composites were ground with a mortar and pestle to a fine powder. The fine powder was weighed and mixed with the 7 wt% PAA binder solution using a ratio of 9:1 (powder PAA). Ethanol was added to reduce the viscosity to an ink-like consistency, then added

to a cupper foil, casting it with a Dr. Blade to a 30 µm thickness. The cast slurry was air dried for 24 hours, then vacuum dried at 100 °C overnight. A slurry of $LiFePO_4$/carbon composites was punched to a ½ inch diameter disk and weighed. The copper foil was subtracted from the material and then multiplied by 90% of active material. This is the mass to be utilized for the electrochemical performance test.

3.3. Battery Preparation and Electrochemical Evaluation

Lithium ion batteries were assembled in the laboratory using coin-type (CR2032) either half-cells or full cells. The half Li-ion cells consisted of a working electrode (anode or cathode) and lithium metal chip as the counter electrode. For the Li-ion full cells, a Lithium metal oxide (LMO) is used as the cathode and CFs or metal-oxide/carbon composite fibers as the anodes. The Li-ion half-cells were assembled in a glove box (Mbraun, Labstarpro) filled with Argon, having a content of <0.5 ppm of O_2 and H_2O. The weight range of the ½ inch anode disk was between 2-5 mg, and was placed in the positive terminal, followed by three drops of electrolyte. A Celgard 2500 separator was then placed above the anode, and ten drops of electrolyte were added. The next step consisted of placing the lithium chip, followed by the stainless-steel spacer, continuing with a spring, and finishing capping with the negative terminal (Figure 9). The cell was then crimped with a MSK-110 hydraulic crimping machine to 80 kg/cm^2.

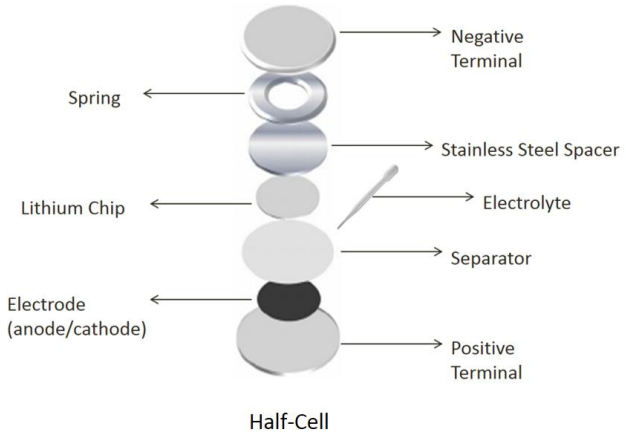

Figure 9: A schematic of the assembly procedure of half-cells [63].

For this work, two different electrolytes were used. The OLE consiting of 1 M $LiPF_6$ in EC/DMC 1:1 v/v ratio and 1 M LiTFSI in 60% EMI-TFSI/ 40 % EC/DMC with an addtion 5 wt% of SN were tested.

Four diffrent experiemtns were used to evalute the eelctrochemcial perforamcne of Li-ion cells, those included the cycle performance, rate capability, cyclic voltromatric, and impedance tests. The cycle performace was evaluated in a charge-discarge test with a voltage window of 0.05 - 3.0 V for anodes, 2.5 – 3.8 V for the $LiFePO_4$ cathode, and 2.5-4.2 V for the $LiCoO_2$ cathode. All electrodes were tested wat a current density of 100 mA/g. Different rate capability tests were perofred using the following curent densities, 50 mA/g, 100 mA/g, 200 mA/g, 500 mA/g, and then again at 50 mA/g. The current density of each electrode is based on the active material's mass. The cyclic voltametry experiemts were performed using a BioLogic BS-100 at a scan rate of 0.2 mV/s between 0.05 and 3 V for the anode, 2.5 and 3.8 V for $LiFePO_4$ cathode, and 2.5 and 4.2 V for $LiCoO_2$ cathode. The impedance experiemtns for all electrodes were

performed using a Metrohm Autolab (PGSTAT128N) (at a frequency range between 0.1 Hz and 1 kHz).

The ionic conductivity of the electrolyte was performed using the following method. The positive terminal was put at the bottom, followed by a stainless steel spacer. It would followed a Teflon washer that is going to be filled with electrolyte, as demonstrated in Figure 10. After the electrolyte is added two stainless steel spacers follow, finishing with a spring and clamping the negative terminal. The resistance was obtained using the Metrohm Autolab (PGSTAT128N) (at a frequency range between 0.1 Hz and 1 kHz) at different temperatures. A heating chamber was assembled by the following method a 12" X 2" X2" rectangular prism copper bar was purchased and cut to a 4" X 2" X2". In the middle of the piece a port of 0.510" by 1.455" was milled to insert the battery. In one of the 2" X 2" sides of the rectangular prism, two 0.0625" holes were drill of 2" deep to insert two thermocouples. On that same side, two 0.25" holes were drill with a depth of 3.75" to insert two heating cartridges. Teflon sheets, making the respective openings and screwing it to maintain the heating block insulated, and then covered the copper rectangular prism. The thermocouples and heating cartridges were connected to the temperature process control CN 7500 purchased from Omega, which communicates to the computer by a RS485 USB converter.

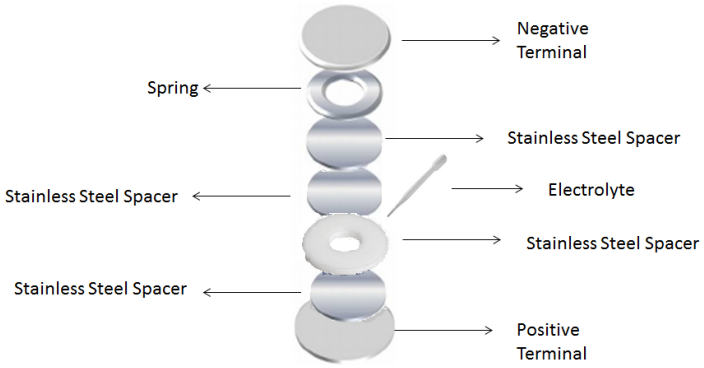

Figure 10: Schematic for a cell preparation to conduct the ionic conductivity test [63].

CHAPTER IV

RESULTS AND DISCUSSION

4.1 Optimization of Electrolyte

Preliminary experiments were conducted in order to determine which electrolytes had a better specific capacity performanc with CFs (Table 1). The concentration of the lithium salt and the mixture of EMI-TFSI was based on literature review which was replicated and confirmed in our laboratory. The CFs cycled with the commercial electrolyte (1 M $LiPF_6$ in EC/DMC (1:1 v/v)) was used as standard in order to determine the electrochemical performance and compare to the different MOILEs with various concentrations of SN. The electrolyte that had the best specific capacity with the least degradation after 100 cycles was 1 M LiTFSI in 60% EMI-TFSI 40% EC/DMC (1:1 v/v) with the addition of 5 wt% of SN. The degradation percent was obtained by dividing the specific capacity at the 100^{th} cycle by the specific capacity of the 2^{nd} cycle and multiplying it by 100.

Electrode analyzed	Lithium Salt Concentration	Lithium Salt	Solvent	SN additive (%)	Degradation (%) after 100 cycles
Carbon Fibers	1 M	$LiPF_6$	EC/DMC (1:1 v/v)	0	2.8
	1 M	LiTFSI	100 % EMI-TFSI	0	82.4
	1 M	LiTFSI	60% EMI-TFSI 40% EC/DMC (1:1 v/v)	0	63.6
	1 M	LiTFSI	60% EMI-TFSI 40% EC/DMC (1:1 v/v)	2	15.4
	1 M	LiTFSI	60% EMI-TFSI 40% EC/DMC (1:1 v/v)	5	2.6
	1 M	LiTFSI	60% EMI-TFSI 40% EC/DMC (1:1 v/v)	10	did not cycle

Table 1: Preliminary results to optimize the MOILE with SN additive.

4.2 Material Characterization

The analyses were conducted to confirm that the results discussed in this paper correlate to CFs, SnO_2/C, $LiFePO_4$/C composite, and commercial $LiCoO_2$ cathode, using the electrolyte proposed. Nuclear Magnetic Resonance (NMR) was used to characterize the chemical composition of the EMI-TFSI. Thermal Gravimetric Analysis (TGA) was used to determine the temperature that the raw polymer carbonizes and CFs under an inert gas. The morphology and structure of fibers were investigated using the Scanning Electron Microscope (SEM) while the energy dispersive spectroscopy (EDS) was used to confirm elemental composition of the fibers.

4.2.1 NMR of EMI-TFSI

The proton (^1H) NMR spectra was obtained by using a Bruker Fourier 300 HD. The following bond are located at the specified peaks: C_2-H at 8.922, C_5-H had a duplicate point at 7.855 and 7.656, CH_2 at 4.4, NCH_3 at 4.035, and t-CH_3 at 1.599. The EMI-TFSI was diluted with protonated acetone, which was also pronounced in the spectra. This peak showed at 2.935. Water impurities were present and had a peak at 2.074 [64, 65].

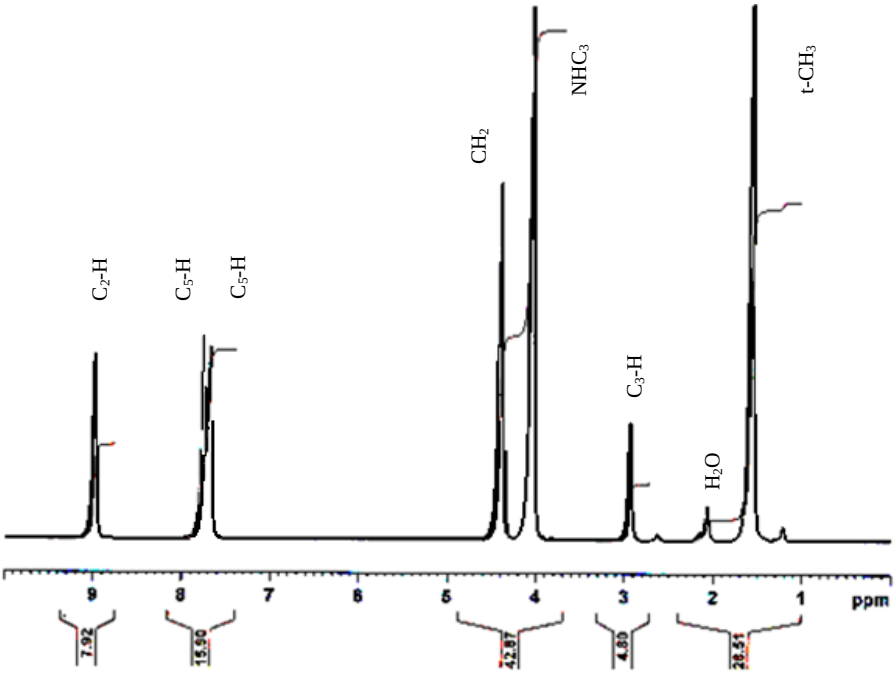

Figure 11: Proton NMR spectroscopy of EMI-TFS.

4.2.2 Carbon Fiber, SnO_2/C Characterization and Comparison

Carbon fiber structure was compared before and after cycling with their respective electrolytes. Figure 12 demonstrates the SEM image of CFs at 20 K, 10 K, and 5 K. It could be observed that at a magnification of 20 K, the surface of the fiber is smooth, non-hollow, and with a diameter of 0.4 µm. At 10 K and 5 K magnification, the fibers show the same consistency. However, the diameter of the fibers seems to vary from 0.5 µm to 3 µm. EDS images were obtained to see the elemental composition of the fibers. The sample holder where the CFs were placed consisted of an Aluminum (Al) and Magnesium (Mg) alloy. The EDS map in Figure 13, demonstrated that the fibers were mainly composed of carbon. The EDS mapping is performed on the area focused. In this sample large amounts of Al and Mg were observed which, is attributed to the sample holders.

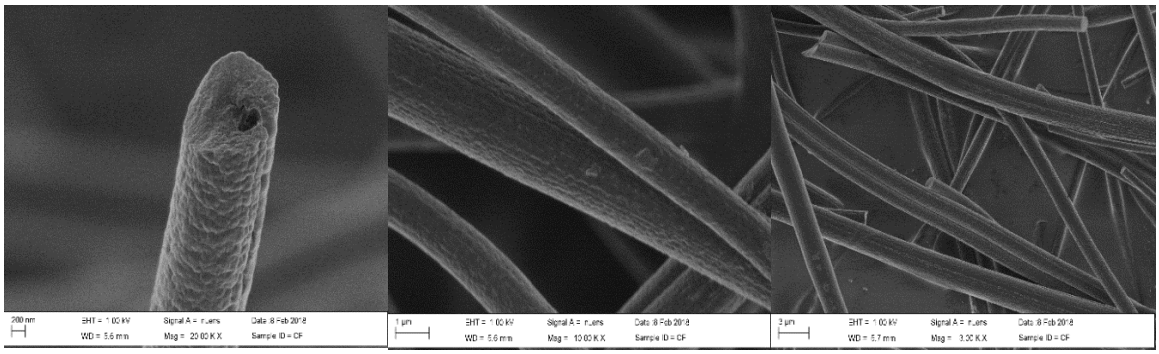

Figure 12: SEM images of uncycled CFs.

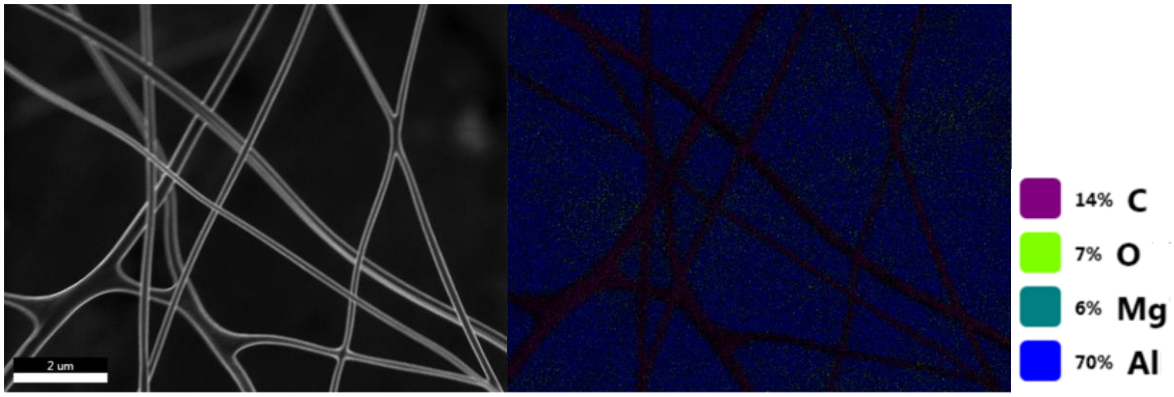

Figure 13: EDAX image of un-cycled CFs.

Figure 14 demonstrates the SEM images of uncycled SnO_2/C fibers at 20 K, 7 K, and 1 K. At 20 K it could be observed that the diameter of the fiber was 0.4 µm. The fiber had a deformation, which could be attributed to Sn agglomerations. When the magnification was zoomed out to 7 K and 1 K the diameter of the fibers seem to vary between 0.5-0.3 µm with the same deformation in most of the fibers. The EDS mapping in Figure 15 shows that the sample contained 49% Carbon, 5% Oxygen, and 6% Tin. The structures of CFs were analyzed before and after cycling with their respective electrolytes. Figure 12 demonstrates the SEM image of CFs at 20 K, 10 K, and 5 K. It could be observed that at a magnification of 20 K, the surface of the fiber is smooth, non-hollow, and with a diameter of 0.4 µm. At 10 K and 5 K magnification, the fibers show the same consistency. However, the diameter of the fibers seems to vary from 0.5 µm to 3 µm. EDS images were obtained to see the elemental composition of the fibers. The sample holder where the CFs were placed consisted of an Aluminum (Al) and Magnesium (Mg)

alloy. The EDS map in Figure 13 demonstrated that the fibers were composed out of carbon, and the AL and Mg content were attributed to the sample holder.

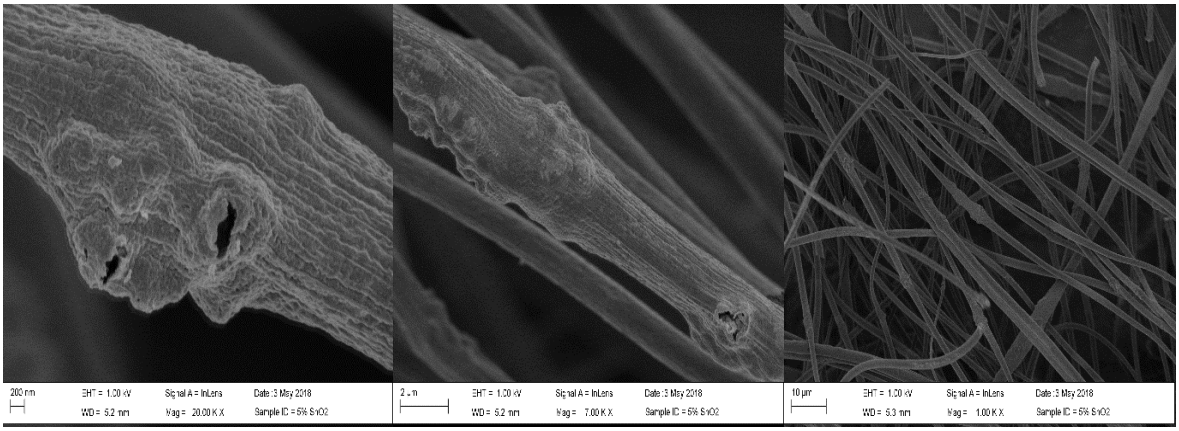

Figure 14: SEM of SnO_2/C uncycled

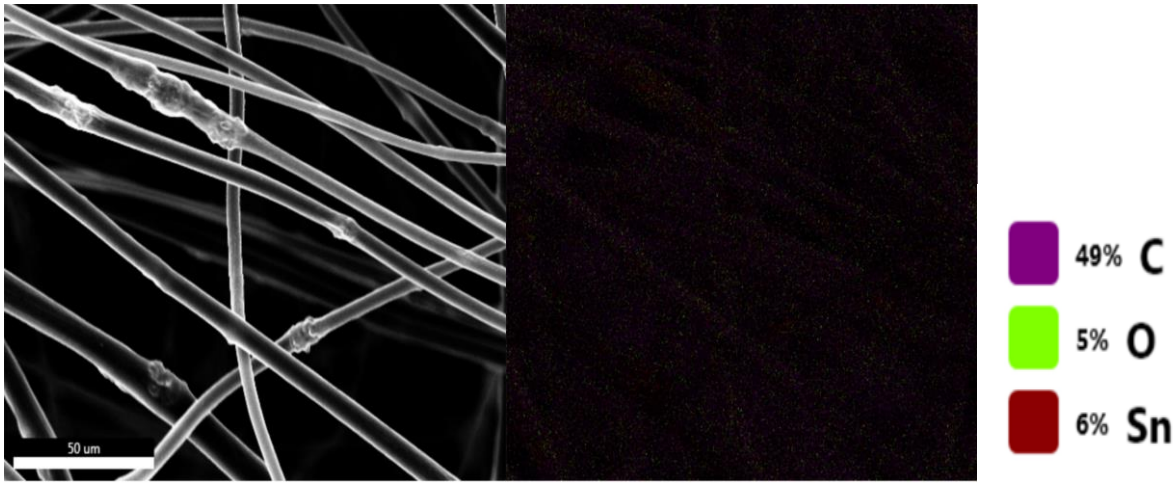

Figure 15: EDS of SnO_2/C uncycled

CFs cycled with 1 M $LiPF_6$ in EC/DMC (1:1 v/v) electrolyte demonstrated in Figure 16 showed to have the same morphology and diameter distribution as the uncycled CFs. At a magnification of 20 K, the fiber seemed to have a residue layer in the surface. When amplifying the magnification at 10 K, a partial coating was observed in the fibers. At a magnification of 5 K partial coating and peaks are observed. The EDS map demonstrated that the CFs were coated with Oxygen, Phosphorous and a minimum trace of Fluorine. The mixture of organic carbonate and $LiPF_6$ decomposes to form the SEI layer. The degradation of the organic carbonate mixture

produces Li_2CO_3, and if water impurities are present, would hydrolyze the $LiPF_6$ to HF [12, 22]. Water impurities could also produce HF formation that could degrade the anode. The SEI layer formation in the CF anode is not uniform with dendrite formation. Uneven coating reduces stability of the cells capacity, and the dendrite formation increases the possibility of puncturing the separator causing a short circuit. Figure 17 shows a 34% of Oxygen, which is attributed to the decomposition of the electrolyte, and 5% Phosphorous from the decomposition of $LiPF_6$.

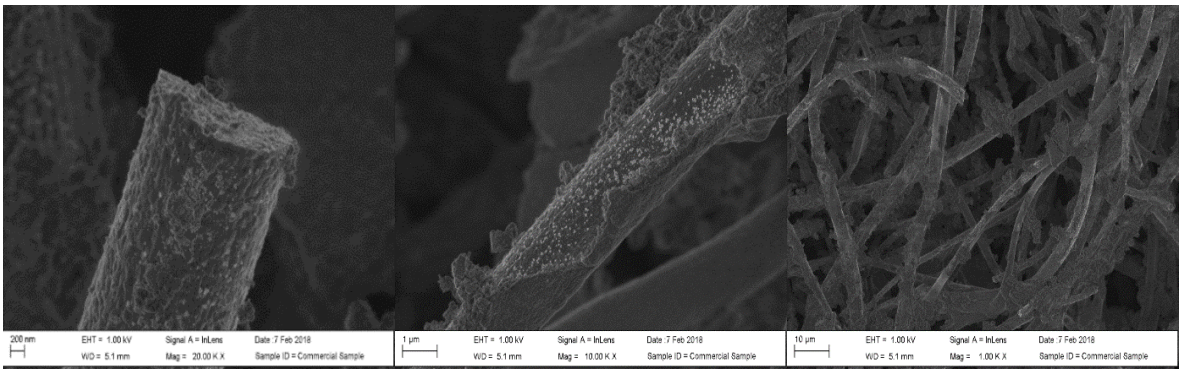

Figure 16: SEM image of cycled CFs with 1 M $LiPF_6$ in EC/DMC (1:1 v/v) electrolyte.

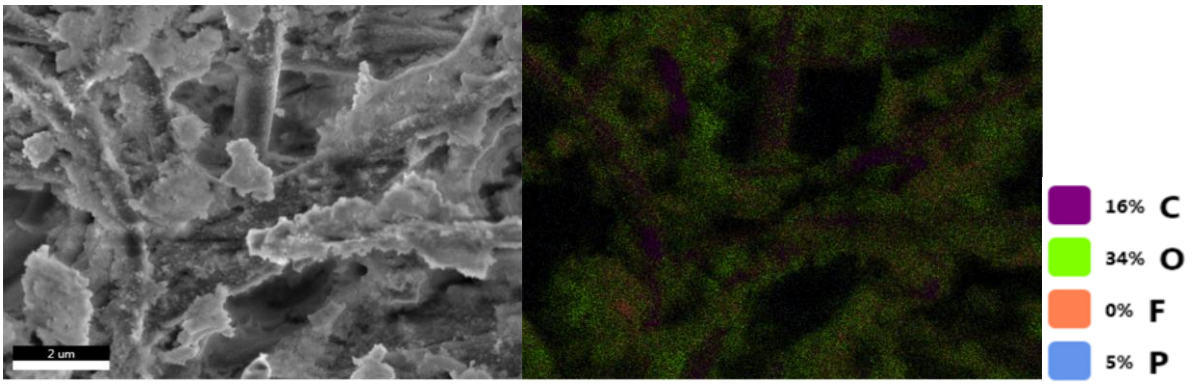

Figure17: EDS elemental mapping of cycled fibers with 1 M LiPF6 in EC/DMC (1:1 v/v) electrolyte.

SnO_2/C anodes were cycled with 1 M $LiPF_6$ in EC/DMC (1:1 v/v) electrolyte. After cycling three images were taken at three different magnifications (Figure 18): at 15K, 4K, and 1K. At 15 K and 4 K magnification, the diameter of the fiber is 1.0 µm, and had a rough surface. In these magnifications, the surface seems to be consistent. However, when the magnification was reduced to 1 K, the surface of the fibers was not consistent, meaning that the SEI formation

did not form uniformly. Nevertheless, the 1 M $LiPF_6$ in EC/DMC (1:1 v/v) electrolyte did not form dendrites, as it did when cycled with CFs (Figure 14). The EDS mapping showed the elemental composition of the SnO_2/C anode after being cycled with 1 M $LiPF_6$ in EC/DMC (1:1 v/v) electrolyte, demonstrated in Figure 19. The elements that were more prominent were Fluorine, Oxygen and Phosphorous. This is due to the decomposition of the solvent and Lithium salt. This is attributed to the SEI layer that was formed on the surface of the fibers.

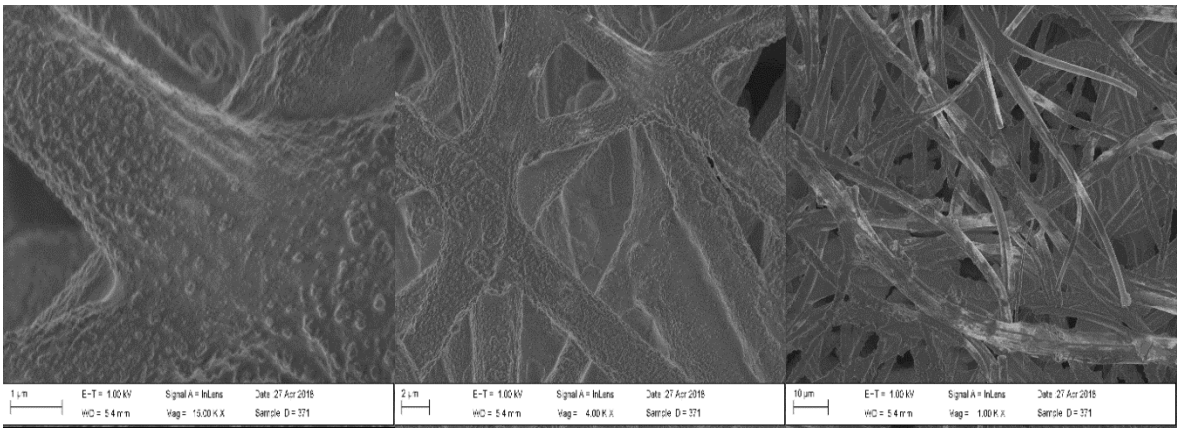

Figure 18: SEM of SnO_2/C anode cycled with 1 M $LiPF_6$ in EC/DMC (1:1 v/v) at 100 mAg^{-1}.

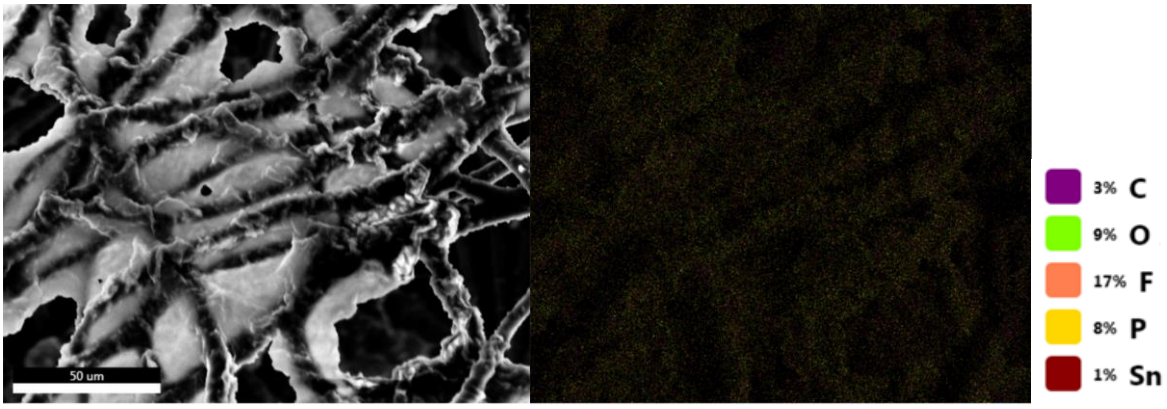

Figure 19: EDS of SnO_2 cycled with *1 M LiPF6 in EC/DMC (1:1 v/v).*

The CF anode cycled with 1 M LiTFSI in 60% EMI-TFSI 40% EC/DMC (1:1 v/v) with the additional 5 wt% of SN, showed in Figure 20, demonstrated that there was a uniform SEI formation on the surface of the fiber. At 20 K magnification, a smooth surface fiber with a

diameter of 0.4 µm fiber. At this magnification, the SEI cannot be observed, but at 10 K and 5 K the layers could be easily observed. Figure 21 shows the EDS mapping demonstrated Oxygen/Sulfur compound on the surface of the fibers. The sulfur was formed due to the EMI-TFSI decomposition and the C-O bonds were formed from EC/DMC (1:1 v/v).

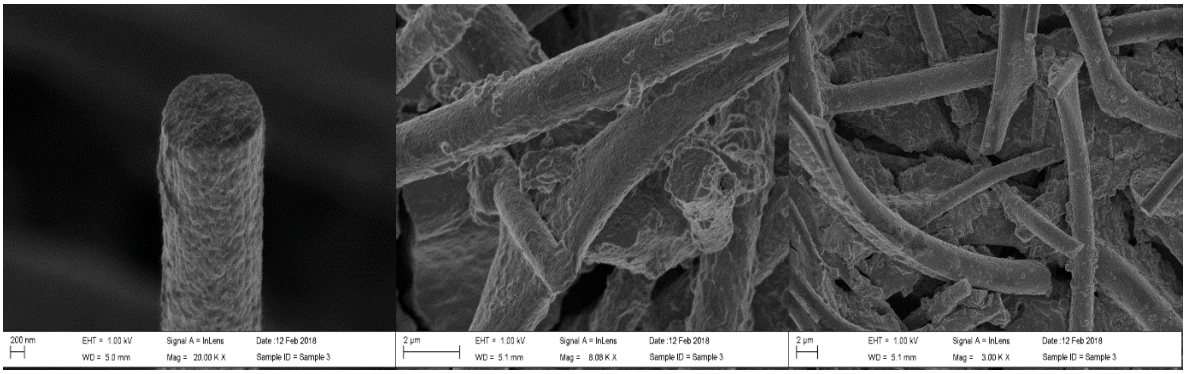

Figure 20: SEM image of cycled CFs with 1 M LiTFSI in 60% EMI-TFSI/ 40% EC/DMC (1:1 v/v) with the addition of 5 wt% SN electrolyte mixture.

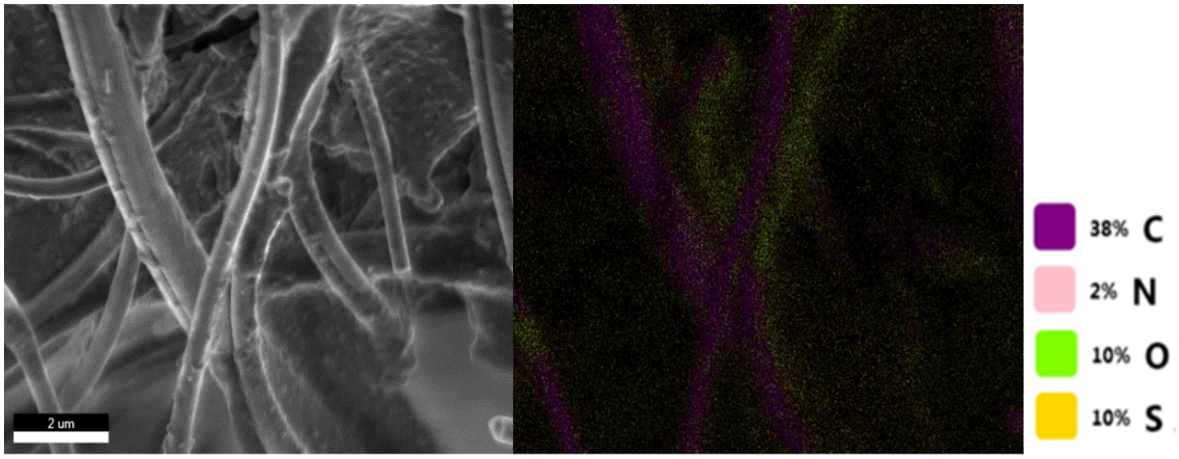

Figure 21: EDS mapping of cycled CFs in a 1 M LiTFSI in 60% EMI-TFSI/ 40% EC/DMC (1:1 v/v) with the addition of 5 wt% SN electrolyte mixture.

The SEM images of SnO_2/C anode were cycled with 1 M LiTFSI in 60% EMI-TFSI 40% EC/DMC with the addition of 5 wt% SN electrolyte. The images obtained are shown in Figure 22. The magnifications used for the images were 5 K, 3K and 1 K. At 5 K and 3K and there is a rough inconsistent surface, with a fiber diameter between 1-3 µm. As the magnification was

zoom out to 1 K, it could be observed that there was no dendrite formation, but there was a residue formed. The EDS mapping analyzed the residue in Figure 23. The elemental mapping concluded that the fibers consisted, mainly, of Carbon and Oxygen; which could be due to the decomposition of the EC/DMC. There were also traces of Tin and Nitrogen. However, this is because the EDS only maps the surface of the material.

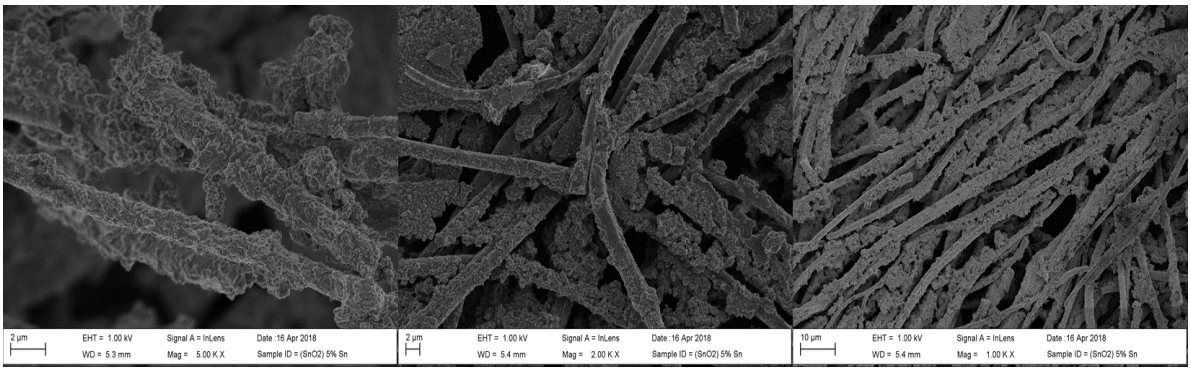

Figure 22: SEM image of SnO_2/C composite cycled with 1 M LiTFSI in 60% EMI-TFSI 40% EC/DMC (1:1 v/v) and 5 wt% SN..

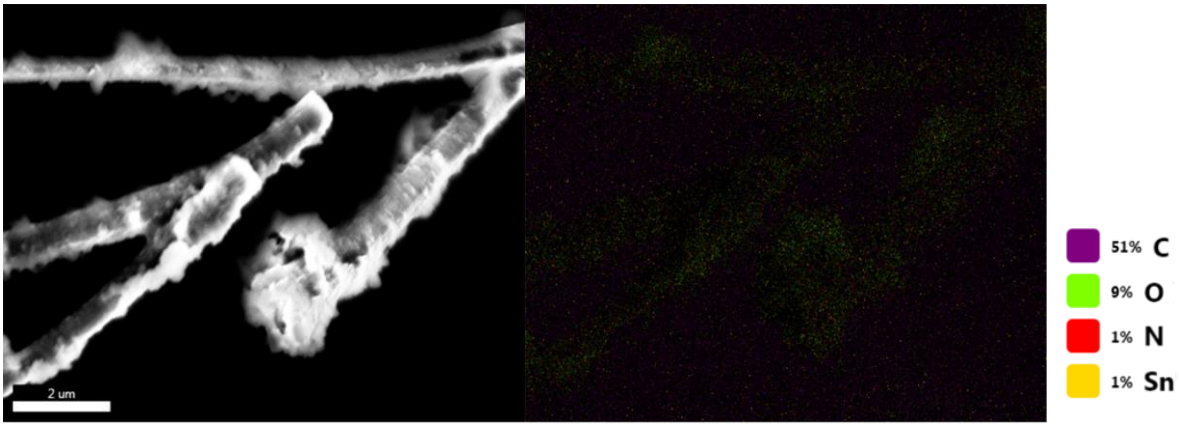

Figure 23: EDS mapping of SnO_2/C fiber composite cycled with 1 M LiTFSI in 60% EMI-TFSI 40% EC/DMC (1:1 v/v) with the addition of 5 wt%.

The XRD characterization of CFs was analyzed using a Bruker D8 DISCOVER Diffractometer X-Ray, at a scan rate of 1 º per minute, using a 2θ angle from 10 to 70. Figure 24 demonstrates the XRD patterns from PAN CFs. A high intensity and broad diffraction peak was

observed at 27.8 º, having no higher order peaks. The intensity is due to the graphitization of the CFs, the absence of high order peaks, and is the result of the amorphous structure of the material.

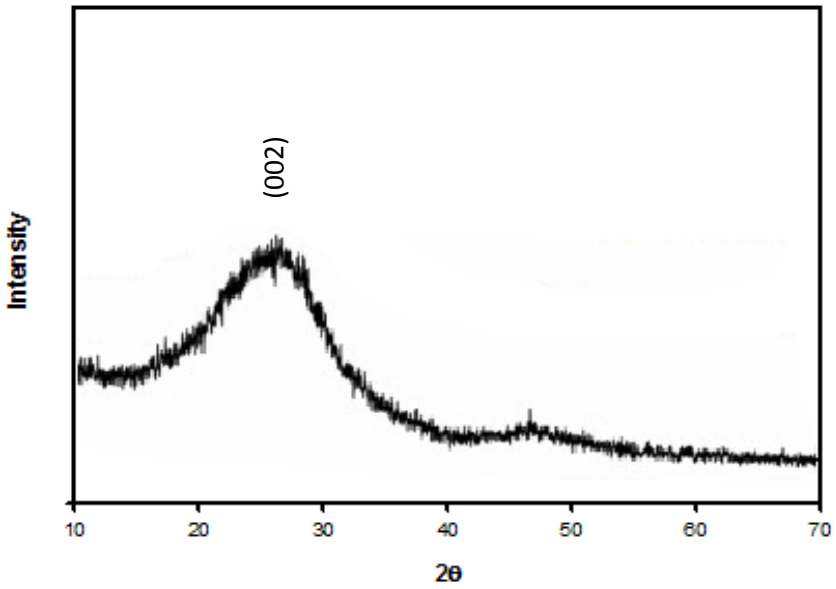

Figure 24: XRD of CFs.

The crystal structure feature of the SnO_2/C anode was analyzed by the XRD with the following parameters, at a scan rate of 1 º per minute, at a 2θ angle from 10 to 70. Figure 25 shows five reflection peaks that appeared in SnO_2/C fiber composite at an angle of 2θ. The predominantly crystalline peaks were (110), (101), (200), (211) and (310). The peaks seemed to overlap five of the seven peaks reflection corresponding to SnO2 crystal structure published by the (JCPDS 41-1445).

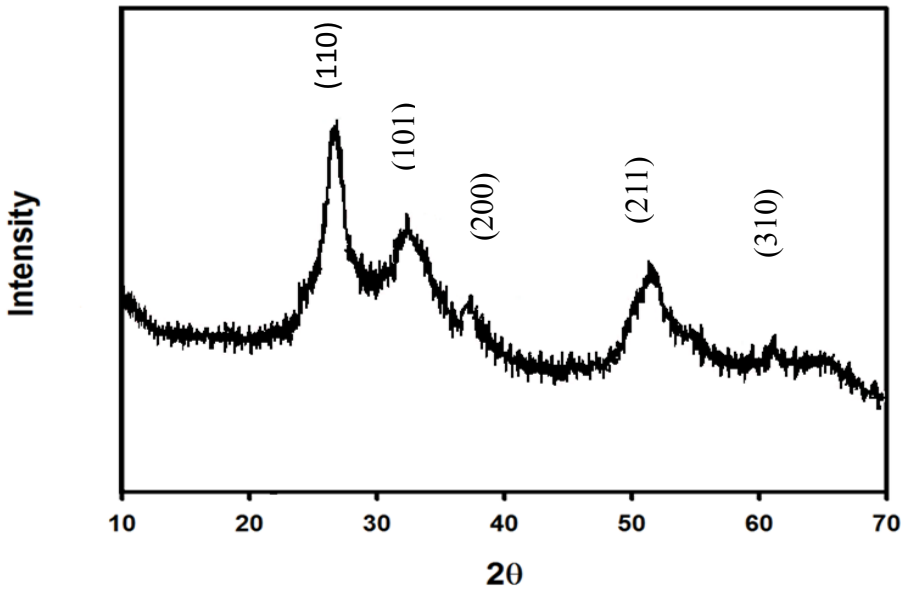

Figure 25: XRD of SnO_2/C fiber composite

TGA was conducted using the TA instruments Q500, with a ramp rate of 10 ºC/minute under inert gas (nitrogen), stopping at a temperature of 800 ºC. The analysis was conducted under inert gas to determine the thermal stability to maximize carbon yield. Figure 26 demonstrates two curves, PAN fibers and carbonized fibers. The behavior of the PAN fibers demonstrated to have a 6 wt% lost when reached a temperature of 110 ºC. At 298 ºC, the nitrile groups started to decompose, leaving C-H bonds. The C-H bonds decomposed after 478 ºC, leaving the C-C backbone structure. The carbon content remaining, after reaching 800 ºC, was 47 wt%. The PAN fibrous mat was carbonized using the method discussed in section 3.2.1, and then a sample that was thermogravimetric analyzed, to observe if any pendant groups were left behind. The carbonized fibers demonstrated to be ~96 wt%, and the 4 wt% could be attributed to moisture that the CFs could have absorbed or any pedant groups left behind [66].

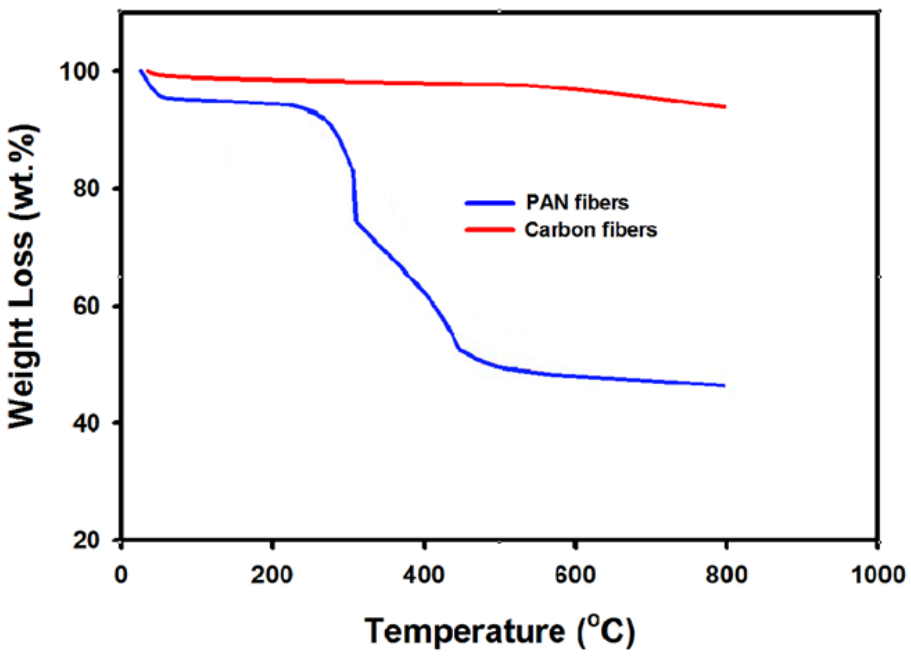

Figure 26: TGA of CFs.

TGA was performed in SnO_2/PAN precursor fibers and SnO_2/C composite fiber (Figure 27). A 4 wt% loss from room temperature to 130 ºC was attributed to the moisture absorbed by the fibers. The second loss step between 360-384 ºC was due to the decomposition of the nitrile pendent group. It is not as pronounced as in PAN fibers, because the addition of SnO_2 increased the decomposition temperature, reducing the amount of polymer. The percentage of SnO_2 in PAN fibers was determined by TGA in nitrogen atmosphere by comparing this sample to PAN fibers. SnO_2/PAN precursor fibers had a third loss step between 384-460 ºC, leaving 57 wt% of SnO_2/C composite. It was compared to the PAN fibers that had a carbon content of 48 wt% after decomposition. The ratio of SnO_2 to carbon was 2:8 respectively. The TGA analysis was also conducted on SnO_2/C composite fiber composites after heat treatment. The graph demonstrates that there was a 3 wt% loss that could be attributed to moisture absorption [67].

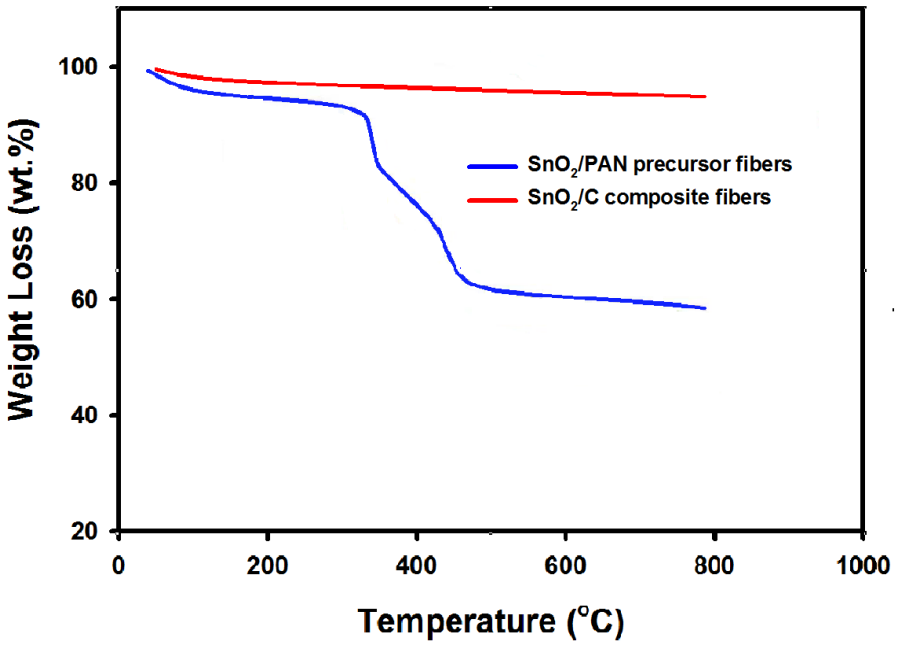

Figure 27: TGA of SnO_2/ PAN precursor fibers and SnO_2/C composite fibers.

4.2.3 $LiFePO_4$/C Cathode Characterization

Figure 28 shows the SEM images of $LiFePO_4$/C cathode after being cycled with 1 M $LiPF_6$ in EC/DMC (1:1 v/v) electrolyte. The magnification at which the images were taken were at 20 K, 5 K, and 1 K. Fibers could not be observed, because it was mortar to fine particles, rather clusters of agglomerate were present. At 20 K magnification, it could be observed that the agglomerates had a diameter range between 0.4-0.8 µm. As the magnification zoomed out to 5 K and 1 K, it could be observed that there was a wide gap between agglomerates. At 1 K, it could be calculated that these gaps are approximately of 10µm. The EDS mapping was taken shown in Figure 29. The elemental composition was of Oxygen and Phosphorous. As mention in previous sections, this is attributed to the SEI formation caused by the decomposition of the organic and lithium salt decomposition.

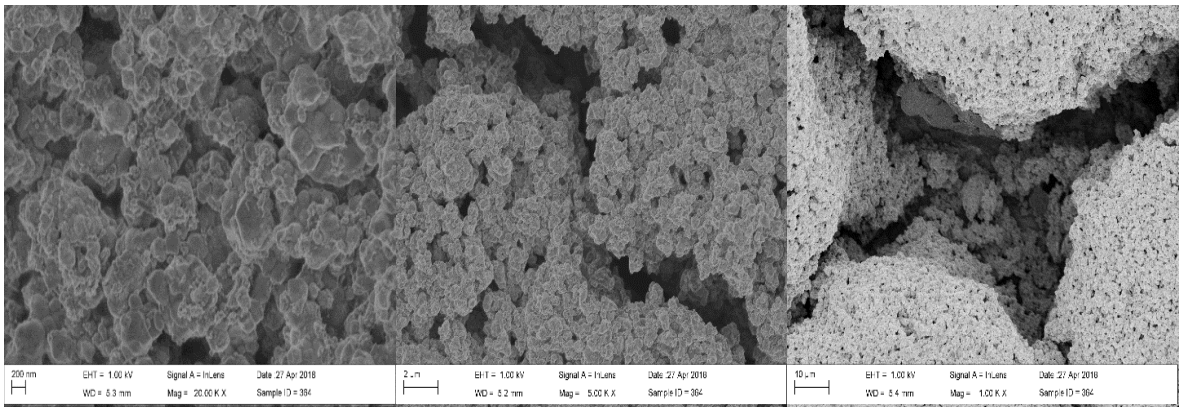

Figure 28: SEM of cycled $LiFEPO_4$/C cathode with 1 M $LiPF_6$ in EC/DMC (1:1 v/v).

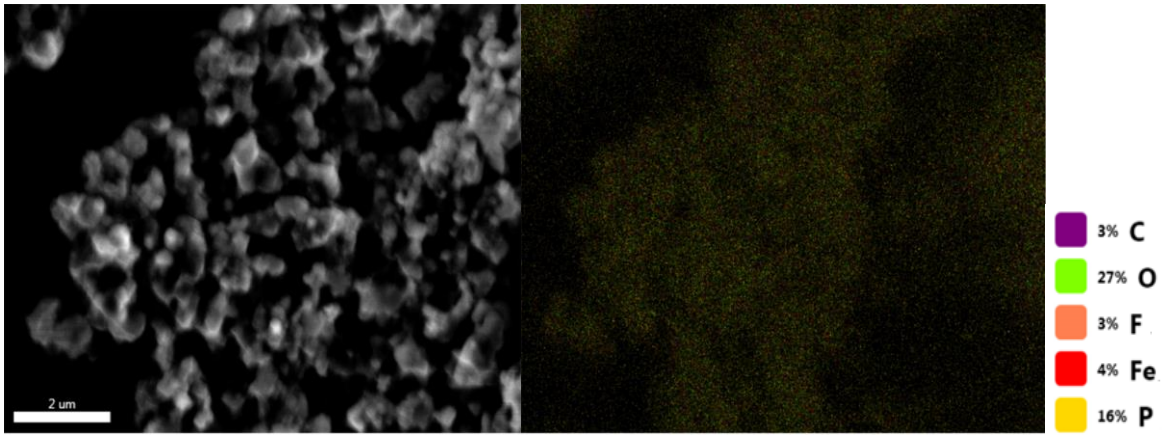

Figure 29: EDS mapping of $LiFePO_4$/C cathode with 1 M $LiPF_6$ in EC/DMC (1:1 v/v).

The XRD peak patterns of $LiFEPO_4$/C cathode were obtained with the following parameters, at a scan rate of 1º per minute, at 2θ angle from 10 to 70 (Figure 30). The peaks reflected appeared at (020), (011), (120), (101), (111), (121), (031), (131), (211), (140), (012), (221), (112), (202), (311), (222), (142), (160) (331), (222), (142), (160) (331), (340), (400), (071), and (133) confirmed by the JCPDS: 40-1499 [68]. The presence of amorphous carbon hump contributed by the carbonized PVP showed in the first degrees.

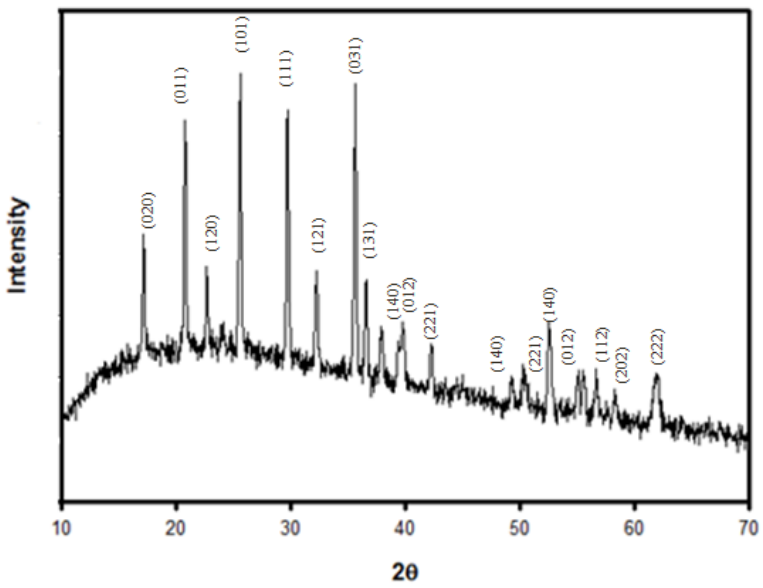

Figure 30: XRD of $LiFePO_4$/C composite.

The TGA experiments were carried out in an inert gas atmosphere (Figure 31). The raw PVP fibers graph showed that it had a 6 wt% of ethanol. It can be concluded that it was ethanol because the weight lost was before 100 ºC, at which water evaporates. The mass was stable from 60 ºC to 450 ºC were the second loss is observed. At this point, the pendent groups were decomposed leaving 37 wt% of carbon at 498 ºC to 800 ºC. The graph of $LiFePO_4$/PVP fibers had the same behavior as the raw PVP, with the only difference being that it had 64 wt% of material that stopped decomposing after 494 ºC. This was due to the mass of $LiFePO_4$ and the carbon backbone. The $LiFePO_4$/C fiber composite was also analyzed and it showed to have small traces of pendent groups since there was a 3 wt% loss after 600 ºC.

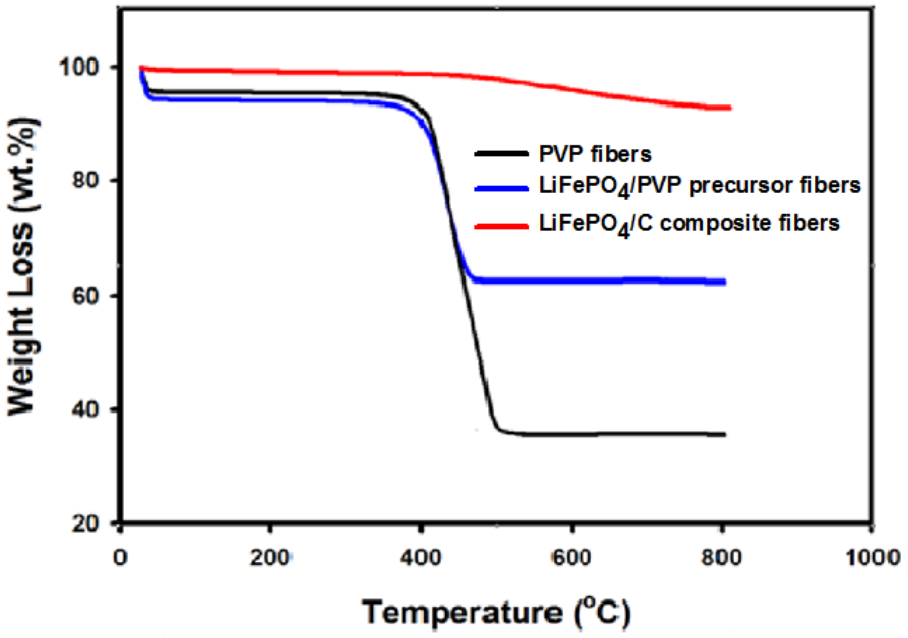

Figure 31: TGA of LiFEPO₄ fiber composite.

4.3 Electrochemical Properties of MOLIEs at Room Temperature

4.3.1 Cycle Performance of CFs in and SnO2/C Fibers

The electrochemical performance of the CFs in Lithium-ion half-cells was investigated using two different electrolytes, Figure 32 shows the galvanostatic charge-discharge profile of the carbon fiber anodes at 100 mAg^{-1}. The CF anode tested with 1 M $LiPF_6$ in EC/DMC (1:1 v/v) electrolyte had an initial discharge capacity (Lithium insertion) of 708 $mAgh^{-1}$ with 73% loss of specific capacity. The CF anode tested with the mixture of 1 M LiTFSI in 60% EMI-TFSI 40% EC/DMC (1:1 v/v) with a 5 wt% of SN. Figure 32 (a), exhibited an initial discharge capacity of 999 $mAhg^{-1}$ in the first cycle and 192 $mAhg^{-1}$ at the second cycle with 53% loss of specific capacity at the first cycle. The loss of the specific capacity is attributed to the SEI formation layer and the decomposition of the electrolyte at the first discharge cycle. The high surface area of the CFs contribute also to the high irreversible capacity at the first cycle. Subsequently, the

fibers that were cycled with the mixture of 1 M LiTFSI in 60% EMI-TFSI, 40% EC/DMC (1:1 v/v) (MOILEs) with an additional 5 wt% of SN exhibited reversible charge capacity of 199 $mAhg^{-1}$ at the second cycle. In contrast, the CFs anode in 1 M $LiPF_6$ in EC/DMC (1:1 v/v) electrolyte exhibited a charge capacity of 148 $mAhg^{-1}$ at the second cycle, increasing to 172 $mAhg^{-1}$ at the 25th cycle where it stabilized indicating a capacity retention of 33% after 100 cycles.

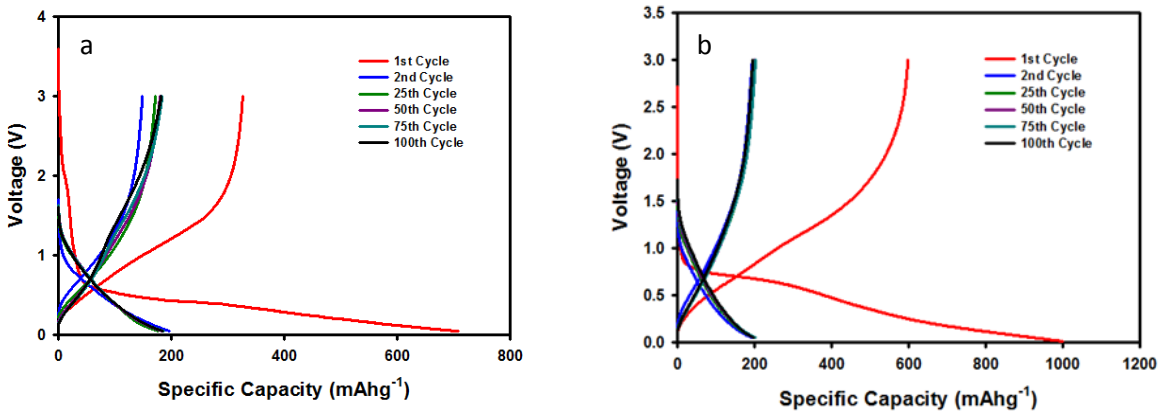

Figure 32: Charge/Discharge profiles for cycled CF anode with 1M LiPF6 in EC/DMC (1:1 v/v) electrolyte (a) and 1 M LiTFSI in 60% EMI-TFSI/ 40% EC/DMC (1:1 v/v) with the addition of 5 wt% SN electrolyte (b).

The cyclic performance experiments were carried out at a current density of 100 mAg^{-1} in a CR2032 coin cell using the two different electrolytes, as observed in Figure 33. The CF anode with 1M $LiPF_6$ in EC/DMC (1:1 v/v) (Figure 33 a) showed an initial specific capacity of 709 mAg^{-1} and a minimum fluctuation capacity at ~185 mAg^{-1}. After 100 cycles, the coulombic efficiency of the cell was 98%. The first cycle had a 46% coulombic efficiency. Similarly, the CF anode in 1 M LiTFSI in 60% EMI-TFSI/ 40% EC/DMC (1:1 v/v) with the addition of 5 wt% SN (Figure 33 b), had a high first initial specific capacity of 999 mAg^{-1}. However, it had highly stable specific capacity of ~205 mAg^{-1} after the second cycle, showing an increased in specific capacity compared to the ~185 mAg^{-1} performed with the 1M $LiPF_6$ in EC/DMC (1:1 v/v)

electrolyte. Upon cycling, the first cycle showed a coulombic efficiency of 60% and was stabilized at ~98% after the second cycle. The improvement of the CF anode in a mixture of 1 M LiTFSI in 60% EMI-TFSI/ 40% EC/DMC (1:1 v/v) with the addition of 5 wt% SN additive is attributed to the formation of uniform SEI layer. This would allow for a uniform insertion and di-insertion of Li ions through the passivation layer of the anode showed in Figure 13 EDS mapping.

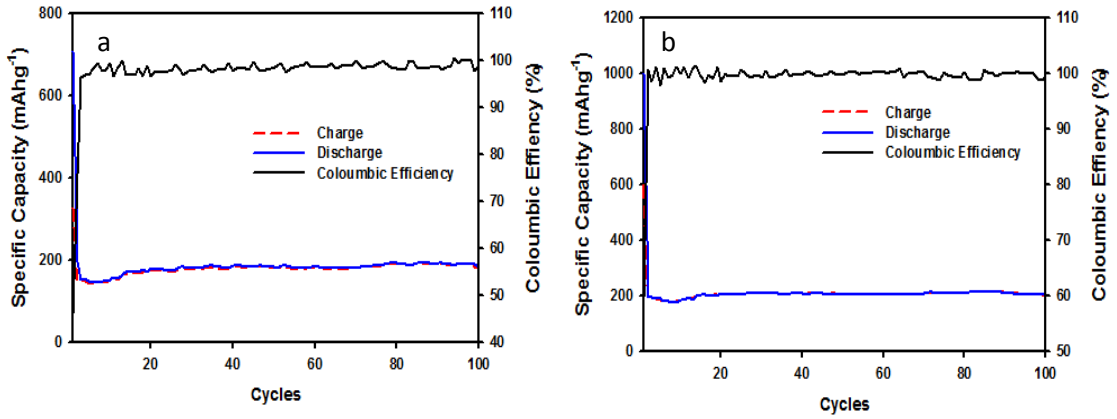

Figure 33: Cycled performance of CF anode in 1M LiPF6 in EC/DMC (1:1 v/v) electrolyte (a) and 1 M LiTFSI in 60% EMI-TFSI/ 40% EC/DMC (1:1 v/v) with the addition of 5 wt% SN electrolyte (b) after 100 cycles with a current density of 100 mAg^{-1}.

The cycle performance of SnO_2/C composite anodes was evaluated by conducing galvanostatic charge/discharge experiments at 100 mAg^{-1} (Figure 34). The SnO_2/C anode in the 1 M $LiPF_6$ in EC/DMC (1:1 v/v) electrolyte showed an initial discharge capacity of 785 $mAhg^{-1}$, which is similar to that of CFs. The reversible specific capacity after 100 cycles was 319 $mAhg^{-1}$.. Nevertheless, the stability of the specific capacity was achieved after the 25th cycle. The CFs showed a stable specific capacity after the 25th cycle (Figure 32 a) indicating a capacity retention of 98%. The volume expansion of SnO_2/C anode after prolonged charge/discharge cycles. Figure 34 b shows the charge/discharge curve at 100 mAg^{-1} of SnO_2/C anode in 1 M LiTFSI in 60% EMI-TFSI 40% EC/DMC electrolyte with 5wt% of SN. The results showed that the first initial

discharge capacity was 934 $mAhg^{-1}$, similar to that of CF anode (Figure 24). However, stability was achieved after the second cycle with a specific capacity of 382 $mAhg^{-1}$, having a ~100% increase compared to the CFs with the same electrolyte (Figure 32), and ~50% increase with the SnO_2/C composite anode cycled with commercial electrolyte.

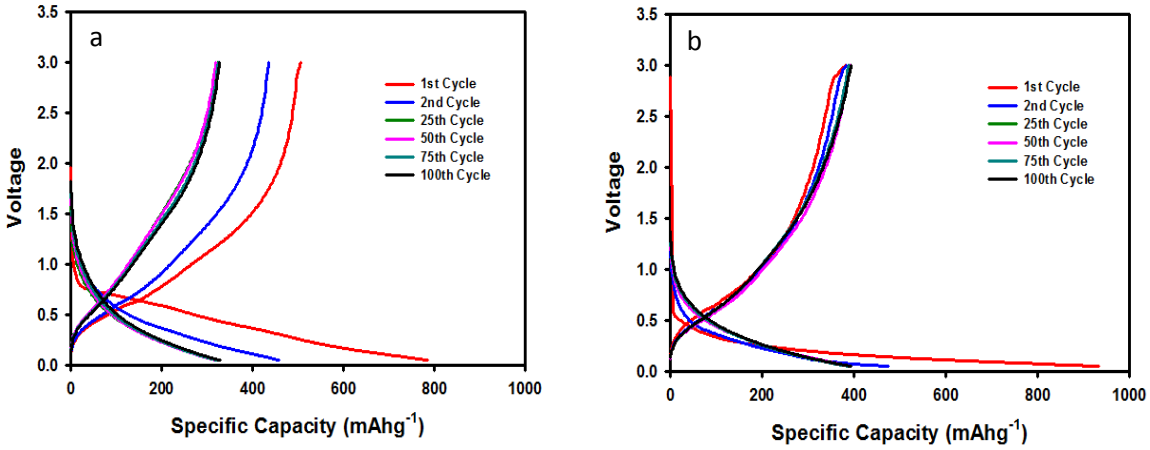

Figure 34: Charge/Discharge profiles for cycled SnO_2/C anode with 1M LiPF6 in EC/DMC (1:1 v/v) electrolyte (a) and 1 M LiTFSI in 60% EMI-TFSI/ 40% EC/DMC (1:1 v/v) with the addition of 5 wt% SN electrolyte (b).

The cycle performance of the SnO_2/C composite anode was evaluated using Li-ion half-cells with organic liquid and MOIL electrolytes (Figure 35). The composite anodes were cycled at a current density of 100 mAg^{-1} for 100 cycles. The performance of the SnO_2/C composite anode in both electrolytes is similar at the first discharge cycle, having a high specific capacity approximately 900 $mAhg^{-1}$. However, the coulombic efficiency of the anode in 1 M $LiPF_6$ in EC/DMC (1:1 v/v) was 64%, compared to that in 1 M LiTFSI in 60% EMI-TFSI 40% EC/DMC (1:1 v/v) with the addition of 5 wt% SN which was 42% . Nevertheless, the capacity of the SnO_2/C anode in the commercial electrolyte (1 M $LiPF_6$ in EC/DMC (1:1 v/v)) was unstable for the first 25 cycles. The capacity of the anode in 1 M LiTFSI in 60% EMI-TFSI 40% EC/DMC

(1:1 v/v) with the addition of 5 wt% SN achieved its stability after the 2nd cycle and with a 50% higher specific capacity than that with the commercial electrolyte.

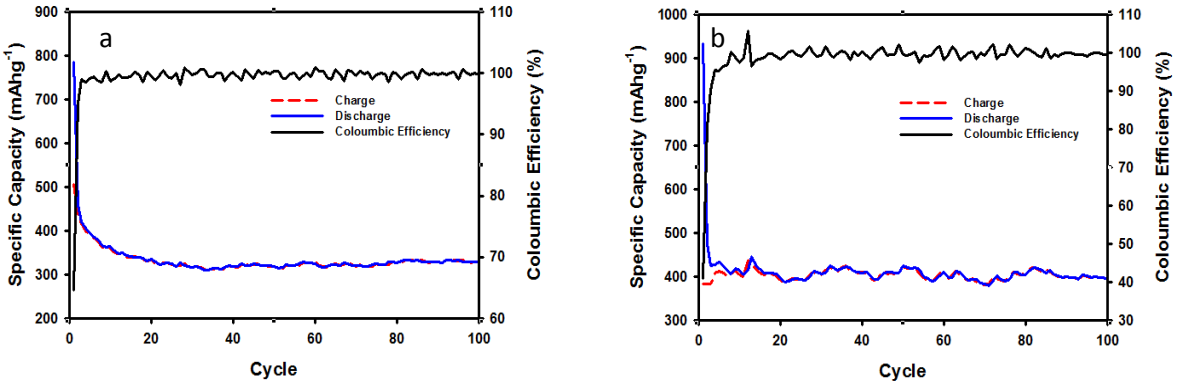

Figure 35: Cycled performance of SnO_2/C fiber anode with 1M $LiPF_6$ in EC/DMC (1:1 v/v) electrolyte (a) and 1 M LiTFSI in 60% EMI-TFSI/ 40% EC/DMC (1:1 v/v) with the addition of 5 wt% SN electrolyte (b) after 100 cycles with a current density of 100 mAg^{-1}.

4.3.2 Rate Performance of CFs and SnO_2/C Fibers

The rate performance of the CF anodes was evaluated at different charge density using the two different electrolytes. The rate capability experiments of CF fibers were carried out using half Li-ion (coin) cells in organic liquid and mixed organic/ionic liquid electrolytes at different current densities of 50 mAg^{-1}, 100 mAg^{-1}, 200 mAg^{-1}, 400 mAg^{-1}, and 500 mAg^{-1}, and 50 mAg^{-1}. In these experiments, 10 charge/discharge cycles at each current density were conducted with a 10-minute rest interval between each rate. After cycling ten times at a current density of 500 mAg^{-1}, the cell was cycled back at 50 mAg^{-1} to observe the recovery performance of the anode. The CFs showed similar performance with both electrolytes, however, CFs in a mixture of 1 M LiTFSI in 60% EMI-TFSI/ 40% EC/DMC (1:1 v/v) and 5 wt% SN (Figure 36 b) showed better performance. The specific capacity of ~286 $mAhg^{-1}$ at a 50 mAg^{-1} curent density than, 1 M $LiPF_6$ in EC/DMC (1:1 v/v) electrolyte had a specific capacity of ~264 $mAhg^{-1}$ (Figure 36 a) at same current density. The specific capacity at a current density of 50 mAg^{-1} with the MOILE

with the addition 5 wt% SN was 8% higher, than the 1 M $LiPF_6$ in EC/DMC (1:1 v/v). The 1 M LiTFSI in 60% EMI-TFSI/ 40% EC/DMC (1:1 v/v) with the addition of 5 wt% SN electrolyte had a higher specific capacity of 21% at 100 mAg^{-1}, 23% at 200 mAg^{-1}, 21 % at 400 mAg^{-1}, and 35 % at 500 mAg^{-1} than the 1 M $LiPF_6$ in EC/DMC (1:1 v/v). The CFs in both electrolytes had an excellent recovery performance comparing the first 10 cycles at 50 mAg^{-1} to the last 10 cycles at the same current density.

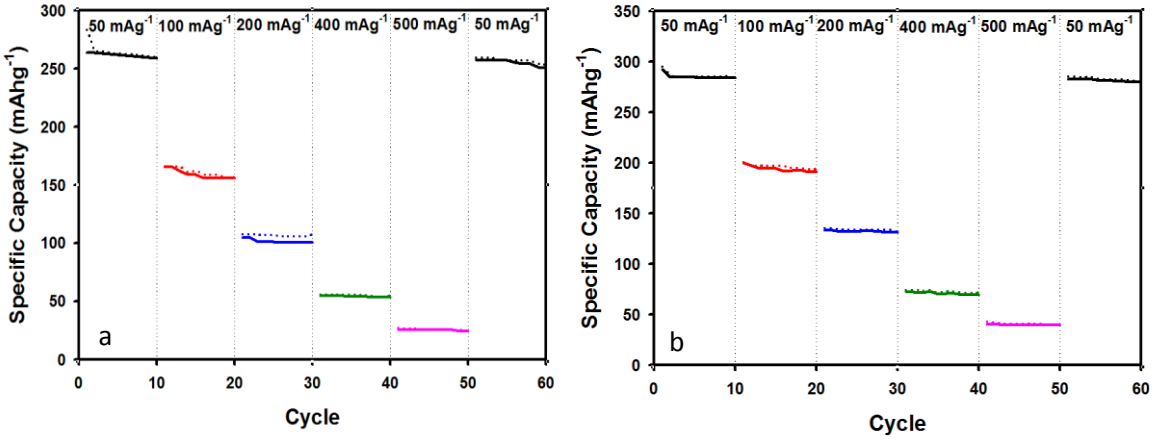

Figure 36:Representation of charge/discharge rate performance of CFs as anode with 1M $LiPF_6$ in EC/DMC (1:1 v/v) electrolyte (a) and 1 M LiTFSI in 60% EMI-TFSI/ 40% EC/DMC (1:1 v/v) with the addition of 5 wt% SN electrolyte (b) at current densities of 50,100,200, 400, 500, and 50 mAg^{-1}.

The rate performance of SnO_2/C composite fibers was further evaluated by conducting current rate (or rate capability tests, rate performance test) experiments of the Li^+ half-cells at different current densities. The SnO_2/C composite fibers were cycled for 10 cycles at various current densities of 50, 100, 200, 400, 500, and then again at 50 mAg^{-1}. This will exemplify the SnO_2/C composite anodes' ability to perform at higher current densities as well as evaluate the capacity recovered after being cycled from a high to low current density. Figure 37 (a and b) shows the rate performance of the SnO_2/C composite fibers anode in organic liquid and MOIL electrolytes. As expected, the composite anodes had higher specific capacity at lower current density and vice versa. At 50 $mAhg^{-1}$, there is a constant decrease in specific capacity ending

with 418 $mAhg^{-1}$ for the cell cycled with the 1 M $LiPF_6$ in EC/DMC (1:1 v/v) electrolyte, and 579 $mAhg^{-1}$ for the 1 M LiTFSI in 60% EMI-TFSI 40% EC/DMC (1:1 v/v) with the addition of 5 wt% SN electrolyte. The decrease in specific capacity of CFs was not present at 50 mAg^{-1}. This can be attributed to the stresses and strains caused by the high volume change of the SnO_2 composite fibers after prolonged charge/discharge cycles. At a current rate of 100 mAg^{-1}, the charge/discharge capacity was stable at ~ 315 $mAhg^{-1}$ for 1 M $LiPF_6$ in EC/DMC (1:1 v/v) and ~441 $mAhg^{-1}$ for 1 M LiTFSI in 60% EMI-TFSI 40% EC/DMC (1:1 v/v) 5 wt% SN. The SnO_2/C composite anode in MOILE and the SN had a higher percentage increase in specific capacity with 25% at 100 $mAhg^{-1}$, 23% at 200 $mAhg^{-1}$, 30% at 400 $mAhg^{-1}$, and 1% at 500 $mAhg^{-1}$, compared to 1 M $LiPF_6$ in EC/DMC (1:1 v/v). However, after cycling back at 50 mAg^{-1}, the SnO_2/C composite fibers with 1 M $LiPF_6$ in EC/DMC (1:1 v/v) had a lower coulombic efficiency than with 1 M LiTFSI in 60% EMI-TFSI 40% EC/DMC (1:1 v/v) and 5 wt% SN [69].

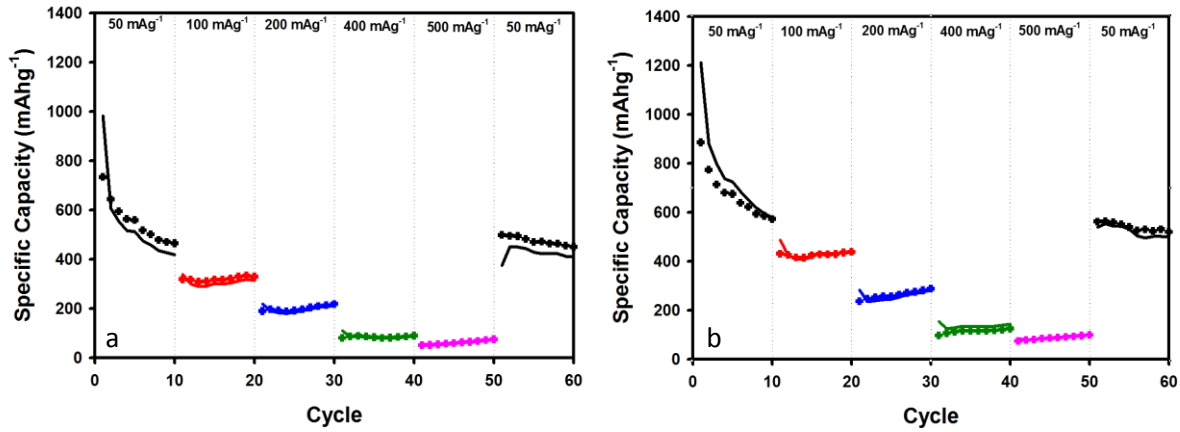

Figure 37: Representation of charge/discharge rate performance of SnO_2/C composite fibers as anode with 1M $LiPF_6$ in EC/DMC (1:1 v/v) electrolyte (a) and 1 M LiTFSI in 60% EMI-TFSI/ 40% EC/DMC (1:1 v/v) with the addition of 5 wt% SN electrolyte (b) at current densities of 50,100,200, 400, 500 and 50 mAg^{-1}.

4.3.3 Cyclic Voltammetry of CFs and SnO_2/C Fibers

The cyclic voltammogram (CV) of the CFs (Figure 38) were carried out at 0.01 mVs^{-1} within potential window of 0.05 V-3 V and evaluated at the first four scans. The interaction of the Li^+ with the CFs demonstrated that the CFs in 1M $LiPF_6$ in EC/DMC (1:1 v/v) electrolyte showed a peak at 0.4 V at the first cycle where the current dropped drastically. This is attributed to the SEI formation at the carbon fiber anode/electrolyte interface. After the first cycle, there was no drop in the current, demonstrating that there were no chemical reactions, prompting only insertion and di-insertion of Li^+ in the CFs. The CV of the CFs with the mixture of 1 M LiTFSI in 60% EMI-TFSI/ 40% EC/DMC (1:1 v/v) with the addition of 5 wt% SN electrolyte demonstrated that at the first cycle, the SEI formation peak was more pronounced which demonstrated the decomposition of the organic solvent and lithium salt.

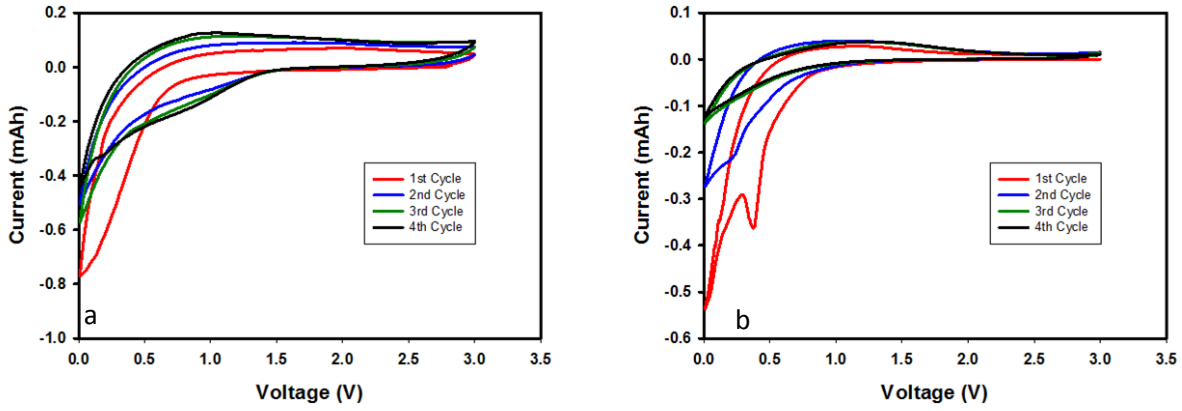

Figure 38: Cyclic voltammetry of CFs cell cycled with 1M $LiPF_6$ in EC/DMC (1:1 v/v) electrolyte (a) and 1 M LiTFSI in 60% EMI-TFSI/ 40% EC/DMC (1:1 v/v) with the addition of 5 wt% SN electrolyte (b)was tested at 0.01 mV/s through 0.05 V and 3V.

The CV experiments of of SnO_2/ Carbon Composite Fibers were performed at a scan rate of 0.1 mVS^{-1} within potential window of 0.05-3.0 V (Figure 39). The first four CV scans were conducted and analyzed. It can be observed that both electrolytes do not show a SEI formation

peak at the first reduction reaction. However, all four cycles showed a peak in the oxidation reaction. The peak in the oxidation at 0.7 V could be attributed to the alloying process of the SnO_2, but during the reduction reaction process (de-alloying), this peak disappeared during the. In addition, there is a peak at 0.2 V at the third and fourth cycles of the SnO_2/ Carbon Composite Fibers in 1 M LiTFSI in 60% EMI-TFSI 40% EC/DMC (1:1 v/v) with 5 wt% SN electrolyte. This could be attributed to the de-alloying process of SnO_2 [70].

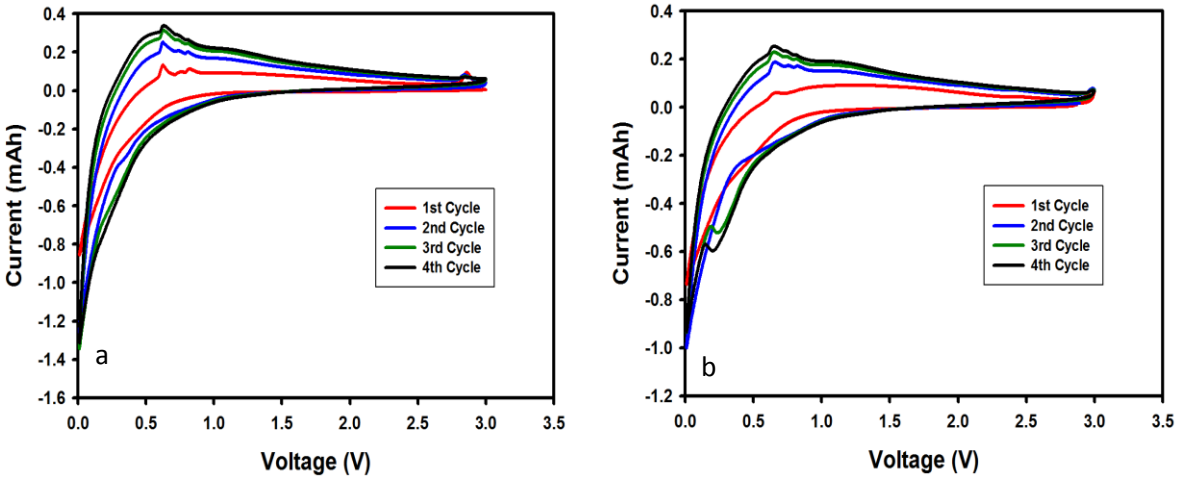

Figure 39: : Cyclic voltammetry of CFs cell cycled with 1M LiPF6 in EC/DMC (1:1 v/v) electrolyte (a) and 1 M LiTFSI in 60% EMI-TFSI/ 40% EC/DMC (1:1 v/v) with the addition of 5 wt% SN electrolyte (b) was tested at 0.01 mV/s through 0.05 V and 3V.

4.3.4 Electrochemical Impedance Spectroscopy of CFs and SnO_2/C Fibers

The electrochemical impedance spectroscopy analysis of the half-cells using CFs as anode was examined using 1M $LiPF_6$ in EC/DMC (1:1 v/v), 1 M LiTFSI in 60% EMI-TFSI 40% EC/DMC (1:1 v/v), and 1 M LiTFSI in 60% EMI-TFSI/ 40% EC/DMC (1:1 v/v) with the addition of 5 wt% SN. The Nyquist plot using a frequency range of 100 kHz-0.1 Hz at an open circuit potential, was obtained before and after cycling (Figure 36). This impedance plot is characterized by a semicircle that represents a charge-transfer resistance of the electrolyte and the electrode. A slope line that represents the diffusion of the Li+ from the electrolyte to the

electrode's surface followed the semicircle. The Nyquist plot was obtained for all three uncycled CFs. However, the half-cell with CFs in the 1 M LiTFSI in 60% EMI-TFSI/ 40% EC/DMC (1:1 v/v) without SN was not cycled, rather, it was used to compare if the addition of SN would reduce the resistance. The use of 1 M LiTFSI in 60% EMI-TFSI/ 40% EC/DMC (1:1 v/v) with the addition of 5 wt% SN as an electrolyte resulted in reduce resistance, compared to the baseline electrolyte without SN. It also demonstrated that the MOILE had less resistance than the organic liquid electrolyte (1M $LiPF_6$ in EC/DMC (1:1 v/v)). Figure 40 shows that after cycling, the diameter of the semicircle increased of CFs in 1M LiPF6 in EC/DMC (1:1 v/v) and 1 M LiTFSI in 60% EMI-TFSI/ 40% EC/DMC (1:1 v/v) with the addition of 5 wt% SN increased compared to that before cycling indicating that there was an increase in resistance. This increase in resistance is attributed to the SEI layer that is nonconductive. The cell cycled with 1 M LiTFSI in 60% EMI-TFSI/ 40% EC/DMC (1:1 v/v) with the addition of 5 wt% SN, had an increase in resistance of 31%. The cell cycled with 1M $LiPF_6$ in EC/DMC (1:1 v/v), had an increment in resistance of 33%. The increase of resistance is attributed to the SEI layer that is nonconductive [71].

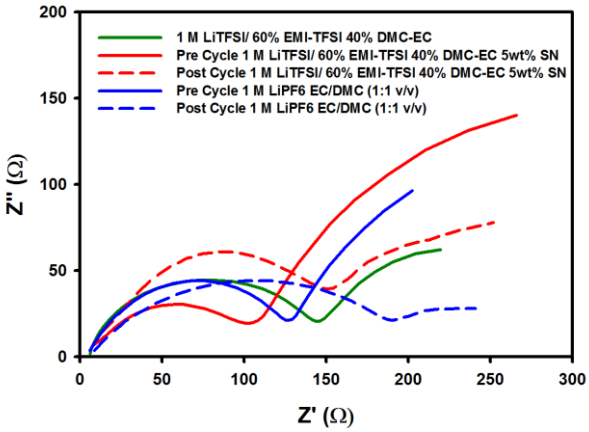

Figure 40: Nyquist impedance plots of cycled and uncycled CFs with 1M LiPF6 in EC/DMC (1:1 v/v) electrolyte, LiTFSI in 60% EMI-TFSI/ 40% EC/DMC (1:1 v/v) electrolyte and 1 M LiTFSI in 60% EMI-TFSI/ 40% EC/DMC (1:1 v/v) with the addition of 5 wt% SN electrolyte.

Figure 41 shows the electrochemical impedance results of SnO_2/C composite fibers before and after cycling with their respective electrolytes. Before cycling, the SnO_2/C composite fibers in both electrolytes had similar interfacial resistance with 4.33 Ωs for 1 M $LiPF_6$ in EC/DMC (1:1 v/v) and 5.25 Ωs in 1 M LiTFSI in 60% EMI-TFSI 40% EC/DMC (1:1 v/v) with 5 wt% SN. However, the resistance of the anode in 1 M LiTFSI with 60% EMI-TFSI 40% EC/DMC (1:1 v/v) and 5 wt% SN was 70 Ωs while the SnO_2/C composite anode in1 M $LiPF_6$ in EC/DMC (1:1 v/v) had a resistance of 105 Ωs . The diffusivity tail of the anode in 1 M LiTFSI in 60% EMI-TFSI 40% EC/DMC (1:1 v/v) with 5 wt% SN was less steep than that with 1 M $LiPF_6$ in EC/DMC (1:1 v/v). After 100 cycles, the resistance of the electrolyte was still similar. Nevertheless, the resistance of SnO_2/C composite fibers increased to 21% using 1 M LiTFSI in 60% EMI-TFSI 40% EC/DMC (1:1 v/v) with 5 wt% SN, and increased 30% using 1 M $LiPF_6$ in EC/DMC (1:1 v/v). The Li^+ diffusivity tail of 1 M $LiPF_6$ in EC/DMC (1:1 v/v) was less than 1 M LiTFSI in 60% EMI-TFSI 40% EC/DMC (1:1 v/v) with the addition of 5 wt% SN.

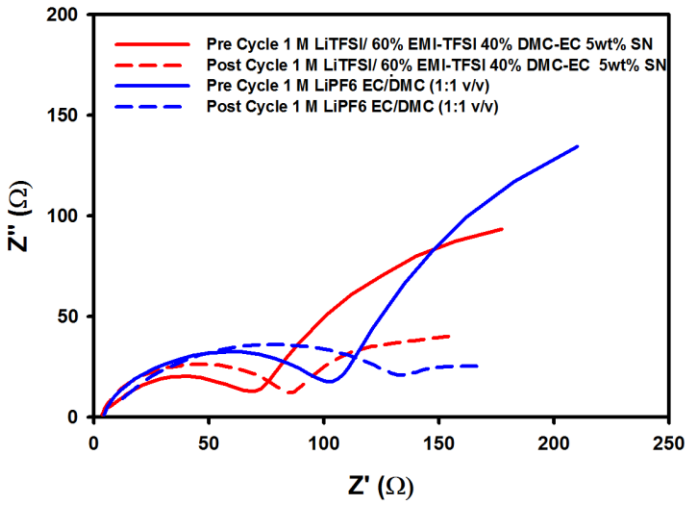

Figure 14: Nyquist impedance plots of cycled and uncycled CFs with 1M $LiPF_6$ in EC/DMC (1:1 v/v) electrolyte, LiTFSI in 60% EMI-TFSI/ 40% EC/DMC (1:1 v/v) electrolyte and 1 M LiTFSI in 60% EMI-TFSI/ 40% EC/DMC (1:1 v/v) with the addition of 5 wt% SN electrolyte.

4.3.5 Cycle Performance of $LiFePO_4$/Carbon Composite Fibers

The working electrode was prepared by mixing active materials with PAA in weight ratio of 9:1. A mixture of $LiFePO_4$/C composite fibers was prepared by milling using N-methyl-2-pyrrolidone as the solvent to form slurry. Then the slurry was coated on Al foil and dried in a vacuum oven at 100 ºC for 24 hours. The electrochemical performance was evaluated using one electrode coin cells (CR2025). For this set of experiments, the electrolyte used was 1 M $LiPF_6$ in EC/DMC (1:1 v/v). The comparison was obtained between the $LiFePO_4$/C composite and commercial $LiFePO_4$. The cells were cycled at 100 mAg^{-1} for 50 cycles, and at a voltage between 2.5 and 4.0 V. Figure 43 a shows results on the commercial electrode on having a stable specific capacity of 154 $mAhg^{-1}$ after 50 cycles. It is observed that there is a voltage plateau at 3.5 V for the charge cycle. This plateau is attributed to the voltage required for the Li^+ to intercalate into the counter electrode. Once the cathode is discharged, there is no more Li^+ to intercalate into the counter electrode, which lead to an increase in voltage. Similarly, for the discharge cycle, there is a voltage plateau at 3.3 V, where the Li^+ are intercalated with the cathode. The cathodic reaction also demonstrated to have high coulombic efficiency between the first charge/discharge cycle. This is attributed to the fact that in the cathodic reaction, there is no electrolyte decomposition. The decomposition happens in the anodic reaction through which the SEI layer is formed. However, when the $LiFePO_4$/C cathode was cycled, it had a first discharge capacity of 135 $mAhg^{-1}$, 13% less than that for the commercial electrode. After the cycles progressed, the specific capacity continued to decrease exponentially, and there was a decrease in voltage between the charge/discharge cycles [68].

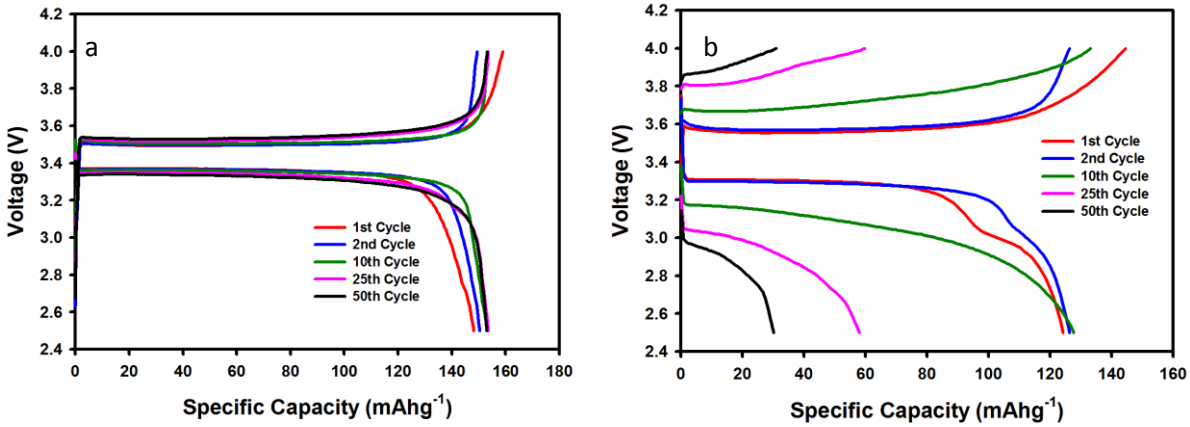

Figure 15: Charge/discharge cycles at 100 mAg^{-1} of commercial LiFePO$_4$ (a) and LiFePO^4/C (b).

Figure 43 shows the cycle performance and coulombic efficiency of the two cathodes. The commercial $LiFePO_4$ had an initial coulombic efficiency of 97%. The specific capacity remained stable from the second cycle at 153 mAhg^{-1}, having a peak at the 29th cycle. This is attributed to a temperature spike occurred over night. The coulombic efficiency of $LiFePO_4$/C cathode was of 88%, having less efficiency than the commercial cathode. The $LiFePO_4$/C fiber composite slurry showed promising results at the first ten cycles with a specific capacity of 137 mAhg^{-1}, exponentially decreased to a specific capacity of 32 mAhg^{-1}.

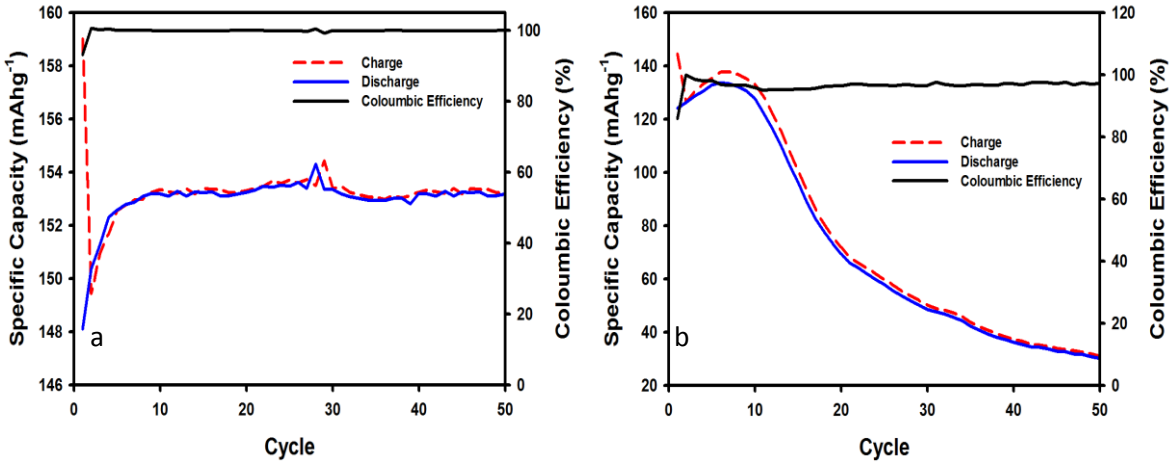

Figure 16: A comparison of cycle performance of LiFePO$_4$/C fiber composite slurry (a) with LiFePO$_4$ commercial slurry (b) with 1 M LiPF6 in EC/DMC (1:1 v/v) electrolyte after 50 cycles with a current density of 100 mAg^{-1}.

4.3.6 Impedance measurements of $LiFePO_4$/Carbon Composite Fiber

Figure 44 displays the Nyquist impedance plot for both $LiFePO_4$/C and commercial $LiFePO_4$. The impedance plot was obtained using the parameters discussed in Section 3.3.1. The impedance plot of the pre-cycled $LiFePO_4$/C cathode was of ~158 Ωs, being higher than that of CFs and SnO_2/C fiber composite (Figures 36 and 41). This is because the $LiFePO_4$ is less conductive than carbon thus higher impedance. $LiFePO_4$ commercial slurry has an impedance of 333 Ωs before being cycled, having a 53% increase. The increase of the impedance in the commercial $LiFePO_4$ slurry could be attributed to a larger percentage of binder used to prepare the electrode. The percent binder used for LiFePO4/C fiber composite slurry was 10%. However, the ratio of active material, conductive carbon, and binder of the commercial $LiFePO_4$ was unknown.

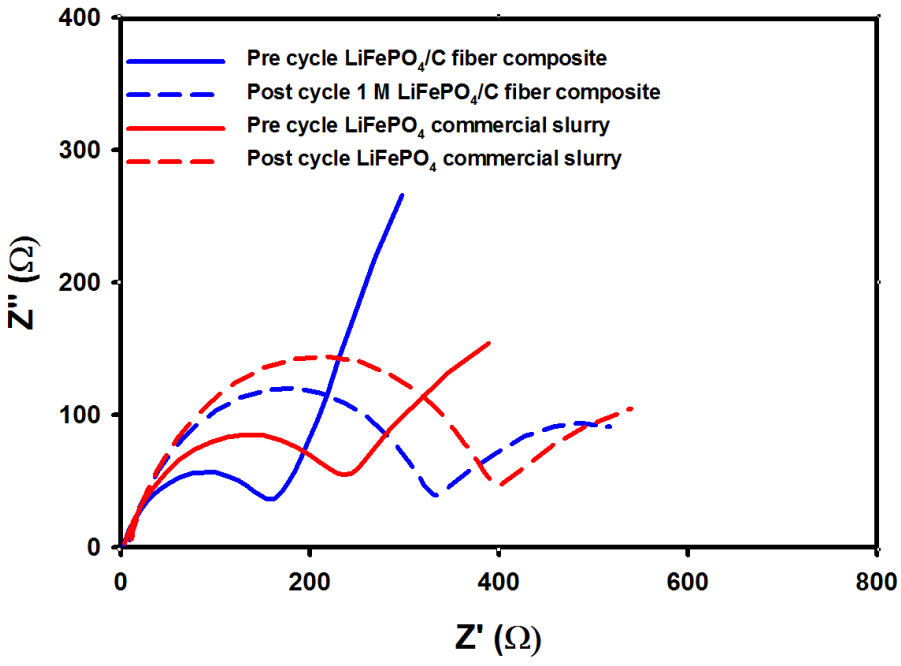

Figure 44: Nyquist impedance plots of $LiFePO_4$/C fiber composite slurry and LiFePO4 commercial slurry, pre and post cycled with 1 M LiPF6 in EC/DMC (1:1 v/v) electrolyte.

4.4 Electrochemical Results at High Temperature

4.4.1 Electrolyte's Ionic Conductivity

The ability for a material to conduct ions through a medium is called ionic conductivity. This is measured using the following equation:

$$\sigma = t/Ra$$

Where σ represents the ionic conductivity which is measured in Siemens per centimeters, *t* the thickness in which the ion has to travel through, R is the resistance of the medium, and *a* is the area that the liquid occupies.

The cells were prepared and tested using the method mentioned in Section 3.2.2, which only calculates the ion diffusivity of the electrolyte at different temperatures. The ionic conductivity of 1 M $LiPF_6$ in EC/DMC (1:1 v/v) is ~0.005 Scm^{-1} at room temperature. Figure 45 shows the ionic conductivity of three mixtures of electrolytes. The electrolyte with 1 M LiTFSI in 100% EMI-TFSI had an ionic conductivity of ~0.006 Scm^{-1} at room temperature. The ionic conductivity increased exponentially as the temperature increased, finishing at 150 ºC with an ionic conductivity of ~0.03 Scm^{-1}. The ionic conductivity for this electrolyte is low compared to the following electrolytes. This is because the viscosity of the IL was high and did not allow for ion diffusivity. As the IL was reduced with the organic carbonates, the ionic conductivity increased. The electrolyte mixture of 1 M LiTFSI in 60% EMI-TFSI 40% EC/DMC demonstrated to have a ~0.014 Scm^{-1}, an increase of 36% compared to 1 M LiTFSI 100% EMI-TFSI (without SN). 1 M LiTFSI in 60% EMI-TFSI 40% EC/DMC with the addition of 5 wt% SN, demonstrated to have the highest ionic conductivity with ~0.026 Scm^{-1} at room temperature. The ionic conductivity increased to ~0.069 Scm^{-1} at 100 ºC. It could be observed that the dilution

of the EMI-TFSI with organic solvents increased the ionic conductivity. However, a small addition of SN also increased the ionic conductivity of the electrolyte.

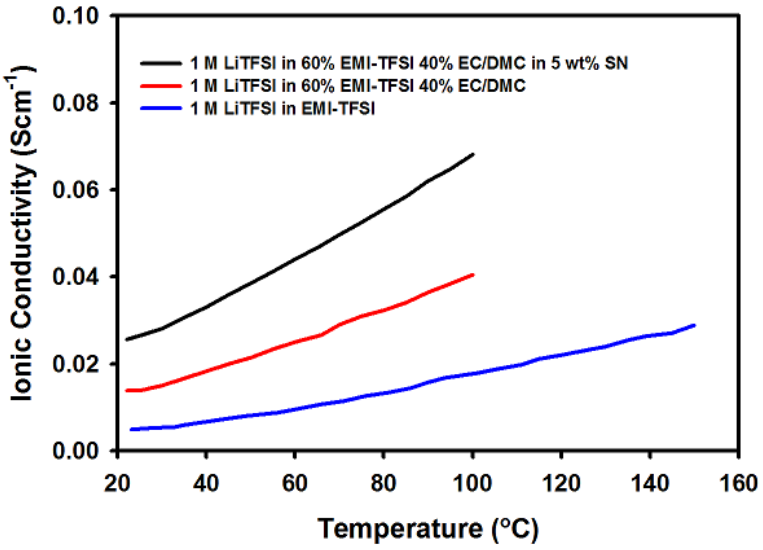

Figure 45: Ionic conductivity of the IL, MOILE, and MOILE with the addition of SN.

4.4.2 Cycle Performance Commercial $LiCoO_2$ Cathode

The charge/discharge curves were obtained using the parameters mentioned in section 3.3.1. The charge/discharge properties of $LiCoO_2$ cathode in the mixed 1 M LiTFSI in 60% EMI-TFSI 40% EC/DMC with and without the addition of 5 wt% of SN were tested at a temperature of 50 ºC for 50 cycles (Figure 46). The specific capacity of commercial LiCoO2 cathode in 1 M LiPF6 in EC/DMC (1:1 v/v) electrolyte at room temperature is 156 $mAhg^{-1}$ [72]. The LiCoO2 cathode cycled with 1 M LiTFSI in 60% EMI-TFSI 40% EC/DMC with and without the addition of 5 wt% of SN had a similar first charge/discharge cycle, with a specific capacity of 150 $mAhg^{-1}$. The first charge/discharge cycle was similar to that of commercial $LiCoO_2$. However, both electrolytes of 1 M LiTFSI in 60% EMI-TFSI 40% EC/DMC without the addition of 5 wt% of

SN, showed a degradation in capacity after the second cycle. The cathode cycled with 1 M LiTFSI in 60% EMI-TFSI 40% EC/DMC (without SN) demonstrated stability for the first ten cycles, then rapidly degraded from a specific capacity of 148 $mAhg^{-1}$ in the 10^{th} at cycle, to a specific capacity of 91 $mAhg^{-1}$ to the 50^{th} cycle. In contrast, the 1 M LiTFSI in 60% EMI-TFSI 40% EC/DMC with the addition of 5 wt% SN, showed the same specific capacity of 150 $mAhg^{-1}$ in the first cycle. After the second cycle, the specific capacity gradually decreased to a specific capacity of 129 $mAhg^{-1}$. The specific capacity degradation of commercial $LiCoO_2$ in 1 M LiTFSI in 60% EMI-TFSI 40% EC/DMC with 5 wt% SN was of 14% loss after 50 cycles. The 1 M LiTFSI in 60% EMI-TFSI 40% EC/DMC (without SN) had a specific capacity loss of 39%. The degradation of the specific capacity of the electrolyte without the additive can be attributed to the decomposition of the organic mixture. The SN additive enhanced thermal stability, reducing the degradation of the organic solvent [19, 20, 73, 74].

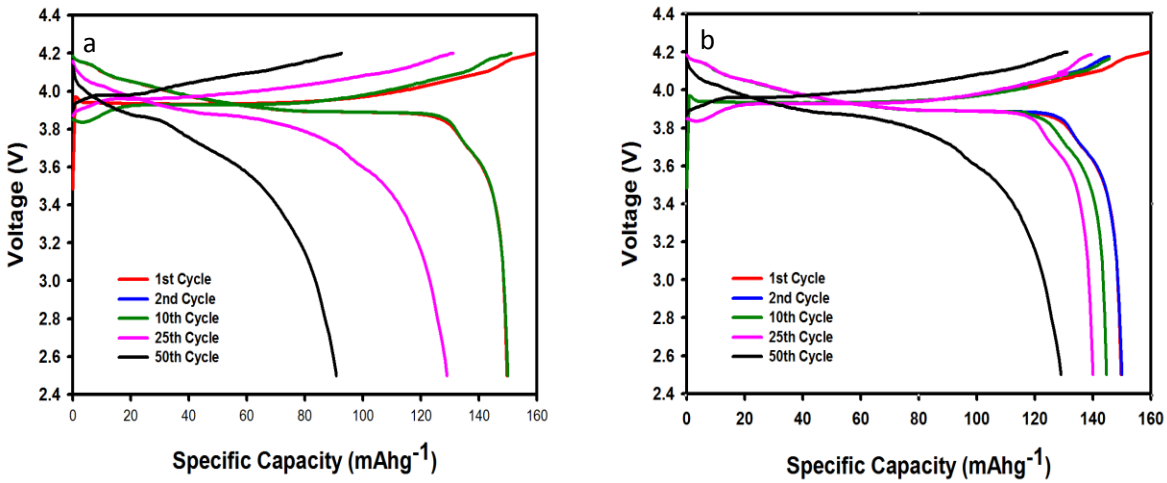

Figure 46: Charge/discharge cycles at 100 mAg-1 of commercial $LiCoO_2$ slurry at 60 ºC with 1 M LiTFSI 60% EMI-TFSI 40% EC/DMC EC/DMC (1:1 v/v)(a) and 1 M LiTFSI 60% EMI-TFSI 40% EC/DMC EC/DMC (1:1 v/v) with the addition of 5 wt% SN (b) electrolytes.

The charge/discharge specific capacity vs cycles of $LiCoO_2$ cathode at 50 ºC for 50 cycles with the two different electrolytes were analyzed. Figure 48 a represents the $LiCoO_2$ cathode cycled with 1 M LiTFSI in 60% EMI-TFSI 40% EC/DMC (without SN). This graph showed a

high coulombic efficiency of 98% for 50 cycles and specific capacity stability between 150-145 $mAhg^{-1}$ for the first 20 cycles. However, the specific capacity stability dropped linearly to 91 $mAhg^{-1}$. The coulombic efficiency of the 1 M LiTFSI in 60% EMI-TFSI 40% EC/DMC with the addition of 5 wt% (48 b) showed to be 98%, a specific capacity stability between 150-148 $mAhg^{-1}$ for the first 10 cycles, linearly degrading until the 30th cycle, and stabilizing at a specific capacity of 129 $mAhg^{-1}$.

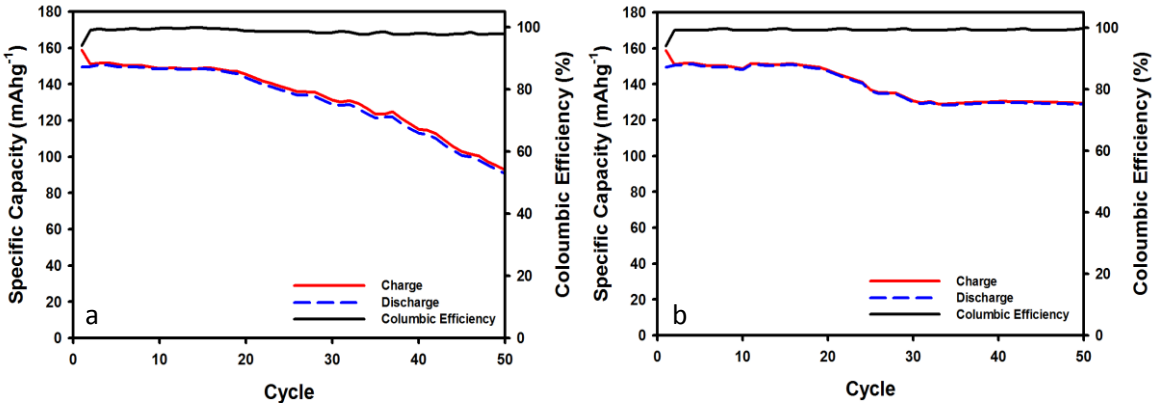

Figure 47: A comparison of cycle performance of $LiCoO_2$ commercial slurry with 1 M LiTFSI in 60% EMI-TFSI 40% EC/DMC (1:1 v/v) electrolyte (a) and 1 M LiTFSI in 60% EMI-TFSI 40% EC/DMC (1:1 v/v) with the addtition of 5 wt% SN electrolyte (b), for 50 cycles with a current density of 100 mAg^{-1}.

CHAPTER V

CONCLUSION

Two different electrolytes (1 M $LiPF_6$ in EC/DMC (1:1 v/v) and 1 M LiTFSI in 60% EMI-TFSI 40% EC/DMC (1:1 v/v) with 5 wt% SN) were synthesized, electrochemically analyzed and compared using two different anodes (CFs and SnO_2/C) that were produced by Forcespinning ® method and subsequent thermal treatment. The electrochemical performance results showed that Li-ion half-cells with carbon fibers in 1 M LiTFSI in 60% EMI-TFSI 40% EC/DMC (1:1 v/v) and 5 wt% SN seem to perform similar to that with CFs in commercial organic liquid electrolyte. Both electrolytes seem to demonstrate good cycling stability, specific capacity, and capacity retention after 100 charge/discharge cycles. The results discussed in this work showed that 1 M LiTFSI in 60% EMI-TFSI 40% EC/DMC (1:1 v/v) with 5 wt% SN had higher ionic conductivity than 1 M $LiPF_6$ in EC/DMC (1:1 v/v) electrolyte. $LiFePO_4$/C composite fibers were also prepared by Forcespinning and subsequent thermal treatment (calcination). The electrochemical performance of the $LiFePO_4$/C composite fibers and commercial $LiCoO_2$ cathode was evaluated at different temperatures using Li-ion half-cells with organic liquid and MOIL electrolytes. The $LiFePO_4$/C composite fibers showed high degradation performance compared to the commercial $LiFePO_4$ and $LiCoO_2$ cathodes. The commercial $LiCoO_2$ cathode was electrochemically evaluated at 50 ºC, cycled with 1 M LiTFSI in 60% EMI-TFSI 40% EC/DMC (1:1 v/v) and 5 wt% SN and had an excellent performance at high in 60% EMI-TFSI 40% EC/DMC (1:1 v/v) and 5 wt% SN showed better electrochemical performance

at room temperature and at 60 ºC compared to that of $LiFePO_4$/C composite fiber and commercial $LiFePO_4$ cathodes and This was attributed to the high ionic conductivity of the MOILE at high temperature.

CHAPTER VI

FUTURE WORK

Electrolytes based on room temperature ionic liquids (RTILs) show promise in addressing the shortcomings of organic liquid, particularly those related to safety. 1 M LiTFSI in 60% EMI-TFSI 40% EC/DMC (1:1 v/v) with the addition of 5 wt% SN electrolyte seems to be a good viable alternative to commercial organic liquid electrolytes. However, the research would have to continue and include different anodes and cathodes with higher energy density. This would not only improve safety of LIBs, but also capacity performance. More work needs to be carried out on evaluating the electrochemical performance of Li-ion full cells with the aim to investigate the effects of additives on the performance and safety of ionic liquid electrolytes at room temperature. Today's batteries have a flammable safety concern and have a limited working temperature range. The full cell batteries could use forcespun metal oxides anodes with different lithium metal oxide cathode materials. The electrochemical tests need to be carried out at different temperatures. Succinonitrile is not the only additive that could improve the electrochemical performance and stability of ILEs Other additives such as propylene carbonate (PC), other carbonates, THF, toluene, acetonitrile (ACN), diglyme and longer oligomers of PEO can also be used to improve the Li ion diffusivity into ILEs.

REFERENCES

1. Kobos, P.H., J.D. Erickson, and T.E. Drennen, *Technological learning and renewable energy costs: implications for US renewable energy policy.* Energy Policy, 2006. **34**(13): p. 1645-1658.

2. Wu, C., et al., *A Review: Enhanced Anodes of Li/Na-Ion Batteries Based on Yolk–Shell Structured Nanomaterials.* Nano-Micro Letters, 2018. **10**(3): p. 40.

3. Xu, K., *Nonaqueous Liquid Electrolytes for Lithium-Based Rechargeable Batteries.* Chemical Reviews, 2004. **104**(10): p. 4303-4418.

4. Tarascon, J.-M. and M. Armand, *Issues and challenges facing rechargeable lithium batteries*, in *Materials for Sustainable Energy*. 2012, Co-Published with Macmillan Publishers Ltd, UK. p. 171-179.

5. Hu, M., X. Pang, and Z. Zhou, *Recent progress in high-voltage lithium ion batteries.* Journal of Power Sources, 2013. **237**: p. 229-242.

6. Castillo, A. and D.F. Gayme, *Grid-scale energy storage applications in renewable energy integration: A survey.* Energy Conversion and Management, 2014. **87**: p. 885-894.

7. Kasnatscheew, J., et al., *Changing established belief on capacity fade mechanisms: thorough investigation of LiNi1/3Co1/3Mn1/3O2 (NCM111) under high voltage conditions.* The Journal of Physical Chemistry C, 2017. **121**(3): p. 1521-1529.

8. Balbuena, P.B. *Electrolyte materials-Issues and challenges*. in *AIP Conference Proceedings*. 2014. AIP.

9. Wang, E., et al., *Stability of lithium ion spinel cells. III. Improved life of charged cells.* Journal of The Electrochemical Society, 2000. **147**(11): p. 4023-4028.

10. Murmann, P., et al., *Investigations on the electrochemical performance and thermal stability of two new lithium electrolyte salts in comparison to LiPF6.* Electrochimica Acta, 2013. **114**: p. 658-666.

11. Agubra, V.A., et al., *ForceSpinning of polyacrylonitrile for mass production of lithium-ion battery separators.* Journal of Applied Polymer Science, 2016. **133**(1).

12. Zhang, S.S., *A review on electrolyte additives for lithium-ion batteries.* Journal of Power Sources, 2006. **162**(2): p. 1379-1394.

13. Mogi, R., et al., *Effects of some organic additives on lithium deposition in propylene carbonate.* Journal of The Electrochemical Society, 2002. **149**(12): p. A1578-A1583.

14. Zhang, S., K. Xu, and T. Jow, *Study of the charging process of a LiCoO2-based Li-ion battery.* Journal of Power Sources, 2006. **160**(2): p. 1349-1354.

15. Zaghib, K., et al., *Lithium-ion cell components and their effect on high-power battery safety*, in *Lithium-Ion Batteries*. 2014, Elsevier. p. 437-460.

16. Ota, H., et al., *Effect of cyclic phosphate additive in non-flammable electrolyte.* Journal of power sources, 2003. **119**: p. 393-398.

17. Lee, H., et al., *The Synthesis of a New Family of Boron- Based Anion Receptors and the Study of Their Effect on Ion Pair Dissociation and Conductivity of Lithium Salts in Nonaqueous Solutions.* Journal of The Electrochemical Society, 1998. **145**(8): p. 2813-2818.

18. Kim, G.-Y., R. Petibon, and J. Dahn, *Effects of succinonitrile (SN) as an electrolyte additive on the impedance of LiCoO2/graphite pouch cells during cycling.* Journal of The Electrochemical Society, 2014. **161**(4): p. A506-A512.

19. Fan, L.Z., et al., *Succinonitrile as a versatile additive for polymer electrolytes.* Advanced Functional Materials, 2007. **17**(15): p. 2800-2807.

20. Kim, Y.-S., et al., *Succinonitrile as a corrosion inhibitor of copper current collectors for overdischarge protection of lithium ion batteries.* ACS applied materials & interfaces, 2014. **6**(3): p. 2039-2043.

21. Wagner, R., et al., *Impact of selected LiPF6 hydrolysis products on the high voltage stability of lithium-ion battery cells.* ACS applied materials & interfaces, 2016. **8**(45): p. 30871-30878.

22. Chen, R., et al., *An investigation of functionalized electrolyte using succinonitrile additive for high voltage lithium-ion batteries.* Journal of Power Sources, 2016. **306**: p. 70-77.

23. Lewandowski, A. and A. Świderska-Mocek, *Ionic liquids as electrolytes for Li-ion batteries—an overview of electrochemical studies.* Journal of Power Sources, 2009. **194**(2): p. 601-609.

24. Fedorov, M.V. and A.A. Kornyshev, *Ionic liquids at electrified interfaces.* Chemical reviews, 2014. **114**(5): p. 2978-3036.

25. Garcia, B., et al., *Room temperature molten salts as lithium battery electrolyte.* Electrochimica Acta, 2004. **49**(26): p. 4583-4588.

26. Wishart, J.F., *Energy applications of ionic liquids.* Energy & Environmental Science, 2009. **2**(9): p. 956-961.

27. Collyer, A.A., *Liquid crystal polymers: from structures to applications*. Vol. 1. 2012: Springer Science & Business Media.

28. Armand, M., et al., *Ionic-liquid materials for the electrochemical challenges of the future.* Nature materials, 2009. **8**(8): p. 621.

29. Ye, Y.-S., J. Rick, and B.-J. Hwang, *Ionic liquid polymer electrolytes.* Journal of Materials Chemistry A, 2013. **1**(8): p. 2719-2743.

30. Jeremias, S., et al., *Polymerizable ionic liquid with state of the art transport properties.* The Journal of Physical Chemistry B, 2013. **117**(36): p. 10596-10602.

31. Nishida, T., Y. Tashiro, and M. Yamamoto, *Physical and electrochemical properties of 1-alkyl-3-methylimidazolium tetrafluoroborate for electrolyte.* Journal of Fluorine Chemistry, 2003. **120**(2): p. 135-141.

32. Wang, M., et al., *Mixtures of unsaturated imidazolium based ionic liquid and organic carbonate as electrolyte for Li-ion batteries.* Electrochimica Acta, 2013. **95**: p. 301-307.

33. Hayano, S., K. Ota, and H.T. Ban, *Syntheses, characterizations and functions of cationic polyethers with imidazolium-based ionic liquid moieties.* Polymer Chemistry, 2018. **9**(8): p. 948-960.

34. Sugimoto, T., et al., *Ionic liquid electrolyte systems based on bis (fluorosulfonyl) imide for lithium-ion batteries.* Journal of Power Sources, 2009. **189**(1): p. 802-805.

35. Li, S.J., et al., *Polymeric Ionic Liquid-poly(ethylene glycol) Composite Polymer Electrolytes for High-Temperature Lithium-Ion Batteries.* Chemelectrochem, 2018. **5**(2): p. 328-334.

36. Kim, H.-T., et al., *Pyrrolinium-based ionic liquid as a flame retardant for binary electrolytes of lithium ion batteries.* ACS Sustainable Chemistry & Engineering, 2015. **4**(2): p. 497-505.

37. Guerfi, A., et al., *Improved electrolytes for Li-ion batteries: Mixtures of ionic liquid and organic electrolyte with enhanced safety and electrochemical performance.* Journal of Power Sources, 2010. **195**(3): p. 845-852.

38. Gélinas, B., et al., *Electrochemical and transport properties of ions in mixtures of electroactive ionic liquid and propylene carbonate with a lithium salt for lithium-ion batteries.* The Journal of Physical Chemistry C, 2016. **120**(10): p. 5315-5325.

39. Forsyth, M., et al., *Inorganic-organic ionic liquid electrolytes enabling high energy-density metal electrodes for energy storage.* Electrochimica Acta, 2016. **220**: p. 609-617.

40. Niedermeyer, H., et al., *Mixtures of ionic liquids.* Chemical Society Reviews, 2012. **41**(23): p. 7780-7802.

41. Seki, S., et al., *Compatibility of N-methyl-N-propylpyrrolidinium cation room-temperature ionic liquid electrolytes and graphite electrodes.* The Journal of Physical Chemistry C, 2008. **112**(42): p. 16708-16713.

42. Fu, L., et al., *Surface modifications of electrode materials for lithium ion batteries.* Solid State Sciences, 2006. **8**(2): p. 113-128.

43. Lee, S., et al., *3D cross-linked nanoweb architecture of binder-free TiO2 electrodes for lithium ion batteries.* ACS applied materials & interfaces, 2013. **5**(22): p. 11525-11529.

44. Li, S. and J. Huang, *A nanofibrous silver-nanoparticle/titania/carbon composite as an anode material for lithium ion batteries.* Journal of Materials Chemistry A, 2015. **3**(8): p. 4354-4360.

45. Zhang, J., et al., *High performance of electrochemical lithium storage batteries: ZnO-based nanomaterials for lithium-ion and lithium–sulfur batteries.* Nanoscale, 2016. **8**(44): p. 18578-18595.

46. Liu, N., et al., *A yolk-shell design for stabilized and scalable Li-ion battery alloy anodes.* Nano letters, 2012. **12**(6): p. 3315-3321.

47. Cui, L.-F., et al., *Carbon− silicon core− shell nanowires as high capacity electrode for lithium ion batteries.* Nano letters, 2009. **9**(9): p. 3370-3374.

48. Wu, Z.-S., et al., *Doped graphene sheets as anode materials with superhigh rate and large capacity for lithium ion batteries.* ACS nano, 2011. **5**(7): p. 5463-5471.

49. Smoukov, S.K., et al., *Scalable Liquid Shear‐Driven Fabrication of Polymer Nanofibers.* Advanced Materials, 2015. **27**(16): p. 2642-2647.

50. Xu, H., et al., *A comparative study of jet formation in nozzle‐and nozzle‐less centrifugal spinning systems.* Journal of Polymer Science Part B: Polymer Physics, 2014. **52**(23): p. 1547-1559.

51. Chiarot, P.R., P. Sullivan, and R.B. Mrad, *An overview of electrospray applications in MEMS and microfluidic systems.* Journal of Microelectromechanical Systems, 2011. **20**(6): p. 1241-1249.

52. Li, D. and Y. Xia, *Electrospinning of nanofibers: reinventing the wheel?* Advanced materials, 2004. **16**(14): p. 1151-1170.

53. Sarkar, K., et al., *Electrospinning to forcespinning™.* Materials Today, 2010. **13**(11): p. 12-14.

54. Agubra, V.A., et al., *Forcespinning: A new method for the mass production of Sn/C composite nanofiber anodes for lithium ion batteries.* Solid State Ionics, 2016. **286**: p. 72-82.

55. McEachin, Z. and K. Lozano, *Production and characterization of polycaprolactone nanofibers via forcespinning™ technology.* Journal of Applied Polymer Science, 2012. **126**(2): p. 473-479.

56. Lu, Y., et al., *Centrifugal spinning: A novel approach to fabricate porous carbon fibers as binder-free electrodes for electric double-layer capacitors.* Journal of Power Sources, 2015. **273**: p. 502-510.

57. Julien, C., et al., *Comparative Issues of Cathode Materials for Li-Ion Batteries.* Inorganics, 2014. **2**(1): p. 132.

58. Guerfi, A., et al., *LiFePO4 and graphite electrodes with ionic liquids based on bis (fluorosulfonyl) imide (FSI)− for Li-ion batteries.* Journal of Power Sources, 2008. **175**(2): p. 866-873.

59. Jin, J., et al., *Li/LiFePO4 batteries with room temperature ionic liquid as electrolyte.* Electrochemistry Communications, 2009. **11**(7): p. 1500-1503.

60. Qiu, L., et al., *Enhanced Cyclability of C/Lithium Iron Phosphate Cathodes with a Novel water-soluble lithium-ion binder.* Electrochimica Acta, 2014. **145**: p. 11-18.

61. Ma, Y.C., Y.B. Yang, and Y.P. Xiong. *Synthesis of triaxial LiFePO4 nanorod with graphite through the electrospinning method*. in *Advanced Materials Research*. 2012. Trans Tech Publ.

62. Zuniga, L., et al., *Multichannel hollow structure for improved electrochemical performance of TiO2/Carbon composite nanofibers as anodes for lithium ion batteries.* Journal of Alloys and Compounds, 2016. **686**: p. 733-743.

63. Birkl, C., et al., *A Parametric Open Circuit Voltage Model for Lithium Ion Batteries*. Vol. 162. 2015. 2271-2280.

64. Hayamizu, K., et al., *Nuclear magnetic resonance studies on the rotational and translational motions of ionic liquids composed of 1-ethyl-3-methylimidazolium cation and bis(trifluoromethanesulfonyl)amide and bis(fluorosulfonyl)amide anions and their binary systems including lithium salts.* Journal of Chemical Physics, 2011. **135**(8): p. 11.

65. Gottlieb, H.E., V. Kotlyar, and A. Nudelman, *NMR chemical shifts of common laboratory solvents as trace impurities.* The Journal of organic chemistry, 1997. **62**(21): p. 7512-7515.

66. Tas, S., et al., *Polyacrylonitrile (PAN)/crown ether composite nanofibers for the selective adsorption of cations.* RSC advances, 2016. **6**(5): p. 3608-3616.

67. Guan, D., et al., *Carbon nanotube-assisted growth of single-/multi-layer SnS 2 and SnO 2 nanoflakes for high-performance lithium storage.* RSC Advances, 2015. **5**(72): p. 58514-58521.

68. Toprakci, O., et al., *Fabrication and electrochemical characteristics of electrospun LiFePO4/carbon composite fibers for lithium-ion batteries.* Journal of Power Sources, 2011. **196**(18): p. 7692-7699.

69. Saha, M.S., R. Li, and X. Sun, *Composite of Pt–Ru supported SnO2 nanowires grown on carbon paper for electrocatalytic oxidation of methanol.* Electrochemistry Communications, 2007. **9**(9): p. 2229-2234.

70. Wang, M., et al., *Hierarchical SnO2/Carbon Nanofibrous Composite Derived from Cellulose Substance as Anode Material for Lithium - Ion Batteries.* Chemistry-A European Journal, 2015. **21**(45): p. 16195-16202.

71. Kim, C. and K. Yang, *Electrochemical properties of carbon nanofiber web as an electrode for supercapacitor prepared by electrospinning.* Applied physics letters, 2003. **83**(6): p. 1216-1218.

72. Ozawa, K., *Lithium-ion rechargeable batteries with LiCoO2 and carbon electrodes: the LiCoO2/C system.* Solid State Ionics, 1994. **69**(3-4): p. 212-221.

73. Matsumoto, H., et al., *Fast cycling of Li/LiCoO2 cell with low-viscosity ionic liquids based on bis (fluorosulfonyl) imide [FSI]−.* Journal of Power Sources, 2006. **160**(2): p. 1308-1313.

74. Zhi, H., et al., *Understanding How Nitriles Stabilize Electrolyte/Electrode Interface at High Voltage.* The journal of physical chemistry letters, 2017. **8**(24): p. 6048-6052.

BIOGRAPHICAL SKETCH

Jahaziel Villarreal is currently residing in 4100 25th St in McAllen, Tx 78504. He was born on September 23, 1987 in Reynosa Tamaulipas Mexico. In 1994 his mother and brothers moved to the United States. He attended La Joya School District where he received his high school diploma in 2006. In that same year he was accepted and attended The University of Texas Pan-American. His Bachelors is in Chemistry, and was obtained in 2013. In 2015 decided to obtain his master's degree in the University Of Texas Rio Grande Valley where he received in 2018.